SYMBOL TIMING ESTIMATION FOR OFDM SYSTEMS

A DISSERTATION

Submitted in partial fulfillment of the requirements for the award of the degree of

MASTER OF TECHNOLOGY

in

ELECTRONICS AND COMMUNICATION ENGINEERING

(With Specialization in Communication Systems)

By

RAVIKUMAR GUGULOTHU

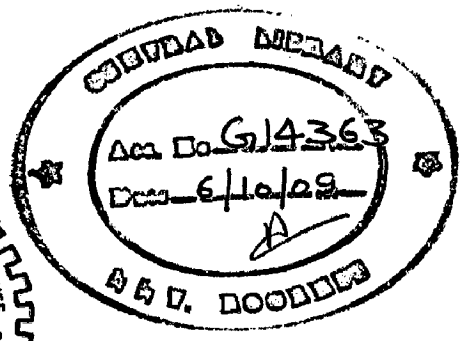

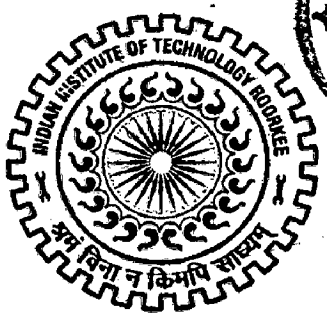

DEPARTMENT OF ELECTRONICS AND COMPUTER ENGINEERING
INDIAN INSTITUTE OF TECHNOLOGY ROORKEE
ROORKEE -247 667 (INDIA)
JUNE, 2009

CANDIDATE'S DECLARATION

I hereby declare that the work, which is presented in this dissertation report entitled, **"SYMBOL TIMING ESTIMATION FOR OFDM SYSTEMS"** towards the partial fulfillment of the requirements for the award of the degree of **Master of Technology** with specialization in **Communication Systems**, submitted in the Department of Electronics and Computer Engineering, Indian Institute of Technology Roorkee, Roorkee (India) is an authentic record of my own work carried out during the period from June 2008 to June 2009, under the guidance of **Dr. ANSHUL TYAGI, Assistant Professor, Department of Electronics and Computer Engineering, Indian Institute of Technology Roorkee.**

I have not submitted the matter embodied in this dissertation for the award of any other Degree or Diploma.

Date: 30-6-2009

Place: Roorkee

RAVIKUMAR GUGULOTHU

CERTIFICATE

This is to certify that the above statement made by the candidate is correct to the best of my knowledge and belief.

Date: 30-6-2009

Place: Roorkee

Dr. ANSHUL TYAGI,
Assistant Professor, E&C Department,
IIT Roorkee,
Roorkee – 247 667 (India).

ACKNOWLEDGEMENTS

First of all, I would like to take this opportunity to extend my heartfelt gratitude to my guide and mentor **Dr. ANSHUL TYAGI**, Assistant Professor, Department of Electronics and Computer Engineering, Indian Institute of Technology Roorkee, who had offered me invaluable support, constructive guidance and helpful discussion throughout my dissertation work. I am grateful for his patience and kindness in answering my questions and revising my submitted reports. Without his continuous encouragement and stimulating suggestions I would have not completed my dissertation work.

I would like to thank all my classmates for their valuable suggestions and comments which made this dissertation work much more clear. I would also like to thank lab assistants **Mr. Mahendra Singh** and **Mr. Anand Krishna Yadav** for their valuable support in completing my work. I want to thank all the people who help me throughout my study at IIT Roorkee.

Finally, I would like to thank my parents and family for their love, trust and encouragement throughout the two years. Without their support, it would have been impossible for me to accomplish what I have accomplished.

RAVIKUMAR GUGULOTHU

ABSTRACT

Robust high data rate wireless communication has several challenges. Transmission of high rate information typically experiences higher delay spread in mobile environments. Furthermore, high mobility introduces time-variations which can make the transmission link less reliable.

Orthogonal Frequency Division Multiplexing (OFDM) is suitable for high delay spread applications. However, performance of OFDM systems, is affected by timing synchronization. Timing synchronization becomes challenging in high mobility applications as power delay profile of the channel can change rapidly due to the sporadic birth and death of the paths. Timing synchronization errors introduce Inter-Carrier-Interference (ICI) in OFDM systems. Furthermore, for mobile applications time-variations in one OFDM symbol introduce ICI as well, which further degrades the system performance. Therefore to have an acceptable reception quality for the applications that experience high delay and Doppler spread, design of robust timing synchronizer is essential. This thesis takes an overall look at this issue.

In this dissertation, we consider symbol timing estimation problem for OFDM systems. OFDM systems are known to be sensitive to time synchronization errors and improving the accuracy of timing offset estimation can help improve the overall system performance. We presented a Maximum-likelihood (ML) estimator method that uses the redundant information within the Cyclic Prefix (CP), which gives the coarse estimation of symbol time offset.

We also discussed the Hybrid ML estimation method, which exploits both the cyclic prefix and the pilot symbols for accurate symbol timing estimation. The performance results of the above discussed methods for AWGN and dispersive channels are simulated in the MATLAB. Simulation results shows that pilot signal design algorithms decrease the variance of the estimate, especially in a time dispersive channel and performs better as compared with the equally spaced pilot signal design algorithms.

LIST OF FIGURES

LIST OF ABBREVATIONS

Additive White Gaussian Noise	AWGN
Bit Error Rate	BER
Band width	BW
Coherence Bandwidth	CB
Channel Estimator	CE
Carrier Frequency Offset	CFO
Channel Impulse Response	CIR
Cyclic Prefix	CP
Digital Audio Broadcasting	DAB
Data Decoding	DD
Data Encoding	DE
Discrete Fourier Transform	DFT
Digital Video Broadcasting	DVB
Frequency Division Multiplexing	FDM
Forward Error Correction	FEC
Fast Fourier Transform	FFT
Guard Interval	GI
Guard Interval Insertion	GII
Inverse Discrete Fourier Transform	IDFT
Inverse Fast Fourier Transform	IFFT
Inter- Symbol Interference	ISI
Inter Channel Interference	ICI
Maximum Correlation	MC
Maximum Likelihood	ML

Minimum Mean Square Error	MMSE
Orthogonal Frequency Division Multiplexing	OFDM
Phase Locked Loop	PLL
Pseudo Noise	PN
Parallel to Serial	P/S
Quadrature Amplitude Modulation	QAM
Quadrature Phase Shift Keying	QPSK
Signal to Noise Ratio	SNR
Serial to Parallel	S/P
Radio Frequency	RF
Wireless Local Area Network	WLAN

TABLE OF CONTENTS

Chapter 1
INTRODUCTION

In today's fiercely competitive environment, information is of extreme importance and there is huge requirement of information at the right place and at the right time. Consequently, Wireless Communication, as a provider for instant information anywhere, has been expanding at a tremendous pace in recent years. With growing number of wireless services and increasing coverage area, the number of users has been growing exponentially, as can be observed from current trends in growing economies like India. As these applications become more sophisticated and widely used, the demand for more bandwidth would increase endlessly.

There has been an increasing demand for high data rate wireless applications in recent years. Digital Audio Broadcasting (DAB), Digital Video Broadcasting (DVB) and Wireless Local Area Networks (WLAN) [1] are a few examples of such applications. The first two applications, while sharing challenges of high speed communications, also require transmission over high mobility links.

Robust high data rate mobile communications have several challenges. Transmission of high rate information typically experiences high delay spread in mobile environments. Furthermore, high mobility introduces time-variations which can make the link less reliable [2].

While current wireless data applications like 802.11a and b are used with limited mobility, ongoing research is working towards making the vision of multimedia high mobility communications a reality. Therefore, a robust design is required to ensure reliable communication in high mobility high delay spread environments as channel estimation, synchronization and data recovery become more challenging [3].

Orthogonal Frequency Division Multiplexing (OFDM) is robust in high delay spread environments and eliminates the need to equalize the effect of delay spread. This feature allows for higher data rates and has resulted in the selection of OFDM as a standard for DAB, DVB and some Wireless Local Area Networks

OFDM as a standard for DAB, DVB and some Wireless Local Area Networks (802.11a). Also, it is being considered as a potential technology for 4^{th} generation mobile communications [1].

Performance of OFDM systems, however, is affected by channel estimation, timing synchronization and mobility. Timing synchronization errors introduce Inter-Channel Interference (ICI). Due to the expansion of symbol length, OFDM systems are very sensitive to ICI. Depending on the choice of the channel estimator (CE), OFDM systems can become even more sensitive to timing synchronization errors. Furthermore, for mobile applications time-variations in one OFDM symbol introduces ICI as well which further degrades the performance. This becomes more severe as mobile speed, carrier frequency or OFDM symbol duration increases. Therefore to have an acceptable reception quality for the application that experience high delay and Doppler spread, design of a robust timing synchronizer, channel estimator and ICI mitigation is essential.

This dissertation takes an overall look at issue of symbol timing synchronization. Timing synchronization in this dissertation refers to the detection of the start of an OFDM symbol [4]. It becomes of great importance and challenge issue in high mobility applications as the power delay profile of the channel can change rapidly due to the sporadic birth and death of the paths.

1.1 Orthogonal Frequency-Division Multiplexing (OFDM)

Orthogonal Frequency-Division Multiplexing (OFDM) is a digital multi-carrier modulation scheme, essentially employing frequency division multiplexing of a large number of closely-spaced orthogonal sub-carriers. Each-subcarrier is modulated with a conventional modulation scheme at a low symbol rate, maintaining data rates similar to conventional single-carrier modulation schemes in the same bandwidth. Its ability to cope with severe channel impairments, like multi-path fading and narrowband interference, without requiring any complex equalization schemes make it superior to single-carrier schemes.

As we already specified that, there has been an increasing demand for high data rate wireless access applications in recent years. Traditionally, such a demand requires more bandwidth. However, due to spectral limitations, it is often impractical or sometimes very expensive to increase bandwidth. So there is a need for effective utilization of spectrum, especially to get higher data rates in available bandwidth. OFDM is one such technique, which will fulfil the above need. OFDM is a multicarrier transmission technique, which divides the single wideband channel into number of parallel narrowband channels called sub-channels; each subcarrier in each sub-channel is being modulated individually by a low rate data stream, generally using some kind of QAM or QPSK [5] digital modulation. We know that in frequency division multiplexing (FDM) technique, lot of spectrum is wasted in the form of guard intervals insertion (GII) between the adjacent channels for channel isolation and filtering purposes. In a typical system, almost half (up to 50%) of the total spectrum is wasted in this manner. This problem becomes worse as the sub-channel bandwidth becomes narrower and total frequency band increases.

But, as mentioned earlier OFDM technique over comes this problem by splitting the available bandwidth into number of parallel narrowband sub-channels. The subcarriers of each sub-channel are made orthogonal to one another, allowing them to be spaced very close together with no overhead (like guard bands), as in FDM. This basic concept of OFDM saving the spectrum is shown in Figure.1.1.

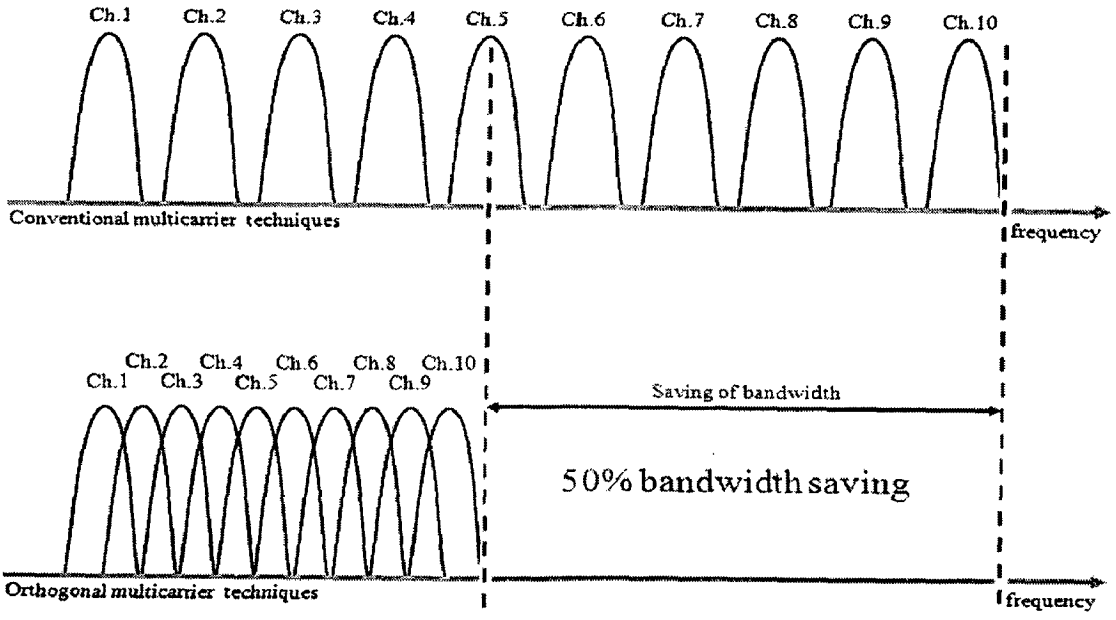

Figure 1.1 Basic concept of OFDM system

The orthogonality of the sub-carriers results in zero cross-talk, even though they are so close that their spectra overlap [5]. Channel equalization is simplified because OFDM may be viewed as using many slowly-modulated narrowband signals rather than one rapidly-modulated wideband signal. Thus, it enables an easy to implement one tap frequency domain equalizer [6]. It should be noted that for designing a receiver with low complexity, it is necessary in an OFDM system that the coherence time of the channel be greater than the duration of one OFDM symbol (i.e., the channel can be considered constant during the symbol). Another requirement is that the coherence bandwidth of the channel be greater than the sub-carrier spacing. OFDM is inherently robust against multi path due to cyclic prefix insertion which helps manage time-domain spreading of the signal minimizing the ISI (Inter symbol interference) effects. It also eliminates the need for pulse-shaping filter.

1.2 Synchronization

Synchronization is an essential task for any digital communication system. Without accurate synchronization, it is not possible to reliably receive the transmitted data [1]. Since it forms the front end of any receiver structure, whole of the receiver architecture depends upon proper synchronization techniques.

Due to the sensitivity difference to various synchronization errors between OFDM systems and single carrier systems, the algorithm design problem has to be approached from the OFDM perspective. The inherent use of Fourier transform techniques allows synchronization techniques and effect of synchronization errors on OFDM systems to be explained using frequency domain tools. Like any other communication system, there is always being a trade-off available between system complexity and performance of the synchronization algorithms.

Synchronization is divided into two subtasks which are called acquisition and tracking. Acquisition consists of coarse estimation or packet detection; carrier frequency offset (CFO) estimation and fine timing. Tracking is related to sampling clock error estimation and residual CFO estimation [7].

Timing Estimation

Timing estimation essentially consists of two main sub tasks: coarse timing estimation or packet synchronization and symbol synchronization or fine timing. Packet detection is the task of finding an approximate estimate of the start of the preamble of an incoming data packet. As such it is the first synchronization algorithm that is performed, so the rest of the synchronization process is dependent on good packet detection performance. For a packet oriented network architecture, finding the packets is obviously of central importance for high network performance. Random access networks do not know exactly when a packet starts. The first task of the receiver in such networks is reliably detecting the start of an incoming packet without prior knowledge. Generally this starting point should be estimated as good as possible, because wrong positioning of the FFT window (e.g. starting point is outside the guard interval (GI)) leads to inter symbol interference (ISI) which also degrades system performance [7] [8]. Actual performance criterion would depend on subsequent synchronization algorithms and preamble design.

Symbol timing, on the other hand, essentially refers to the task of finding the precise starting and ending point of individual OFDM symbols. The symbol timing result defines the IFFT/DFT window; i.e., the set of samples which would be used to calculate IFFT/ DFT of each received OFDM symbol [9] [10]. The frequency domain data is then used to demodulate the sub-carrier of the symbol. The approach to symbol timing is different for WLAN and broadcast OFDM systems. A WLAN receiver cannot afford to spend any time beyond the preamble to find the symbol timing, whereas a broadcast transmission receiver can spend several symbols to accurate symbol timing estimate.

1.3 Motivation

As mentioned in previous sections of this chapter, OFDM is highly sensitive to synchronization errors. Several approaches have been proposed to estimate time and frequency offsets either jointly or individually. In [11] [12], a maximum likelihood (ML) estimator using the redundant information within the cyclic prefix is presented. Due to this inherent structure of OFDM symbols, the estimator requires

no additional pilot symbols. In multipath channels, the cyclic prefix is usually affected by the inter-symbol interference (ISI). So the result of the ML estimator is highly dependent on the channel conditions. To avoid this problem in timing estimation, Schmidl and Cox [13] proposed a correlation estimator using a training symbol with two identical halves. The major drawback of this method is that the timing metric inherently exhibits a plateau around the correct timing point and this plateau would cause a large variance of timing estimation. To overcome this shortcoming, Minn, Zeng, and Bhargava [14] proposed two timing estimation methods to reduce the uncertainty due to the timing metric plateau. Alternatively, a hybrid timing estimation method exploiting both the cyclic prefix and the pilot symbol used for channel estimation is proposed in [15].

Motivated by the fact that synchronization, which is one of the most essential parts of any OFDM based system, is still an open ended topic in recent years OFDM technology based systems, this dissertation work is aimed at studying the performance of symbol timing estimation algorithms. Further, the dissertation work aims to study the different pilot signal design algorithms for efficient symbol time offset estimation, whose performance allows for a tight design of the cyclic prefix improving the spectral efficiency of the system.

1.4 Organization of the Report

The rest of this thesis is divided into the chapters and organized in the following way:

Chapter 2 provides a theoretical concept of bit error rate (BER) Sensitivity of OFDM systems to time synchronization error. Also it includes the effect of timing offset and the existing techniques for timing synchronization.

Chapter 3 includes a brief discussion of various symbols timing estimation schemes available in the literature. Both Cyclic Prefix (CP) based Maximum-likelihood (ML) estimator and the hybrid ML symbol time offset estimator which exploits both redundancy in the cyclic prefix and the pilot symbols for efficient symbol time offset estimation.

Chapter 4 discusses the performance and simulation results of the symbol timing estimation algorithms discussed in chapter 3, for Additive white Gaussian noise (AWGN) channel and the time-dispersive channel.

Chapter 5 provides the conclusion and future work.

Chapter 2

BIT ERROR RATE (BER) SENSITIVITY OF OFDM SYSTEMS TO TIME SYNCHRONIZATION ERROR

As mentioned earlier, the orthogonal nature of the subcarriers in OFDM allows the subcarrier spectra to be densely packed in the frequency domain, i.e., overlapping subcarrier spectra, still realizing the demodulation of the data carried by each subcarrier without any inter-carrier-interference (ICI). Spectral efficiency and multipath immunity are two major feature of the OFDM technique. A major drawback of OFDM is its relatively high sensitivity to time synchronization error, compared to a single carrier system [6]. It is shown that OFDM system incorporating a cyclic prefix (CP) has an asymmetric effect on the received constellation with synchronization error away from CP introducing inter- symbol-interference (ISI), while that towards the CP introducing only a phase error [16]. Time synchronization error refers to the incorrect timing of OFDM symbols at the demodulator introducing ISI, which will affect the bit error rate (BER) of the OFDM system. Cyclic prefix is a redundant part added to each OFDM symbol to increase the multi path immunity

2.1 OFDM Signal Model

The block diagram of a typical OFDM system is shown in Figure 2.2 [3]. The transmitter section converts digital data to be transmitted, into a mapping of sub-carrier amplitude and phase. It then transforms this spectral representation of the data into the time domain using an Inverse Discrete Fourier Transform (IDFT). A copy of the last N_g samples (where N_g is the length of the Cyclic Prefix) is prefixed to obtain an OFDM symbol, which is shown in Figure 2.1. The digital data is then converted to an analog waveform. In order to transmit the OFDM signal the calculated time domain signal is then up-converted to the required transmit frequency.

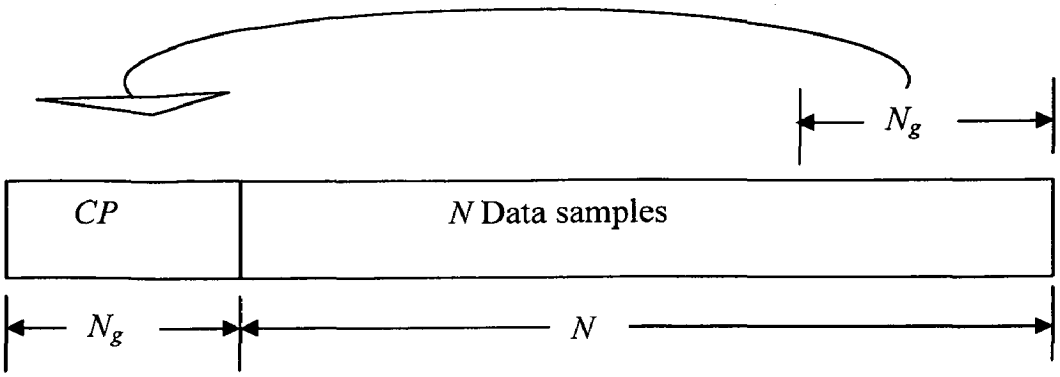

Figure 2.1 OFDM Symbol with cyclic prefix of length N_g

The receiver performs the reverse operation of the transmitter, mixing the RF signal to base band for processing, then using a Fast Fourier Transform (FFT) to analyze the signal in the frequency domain. The amplitudes and phases of the sub-carriers are then picked out and converted back to digital data.

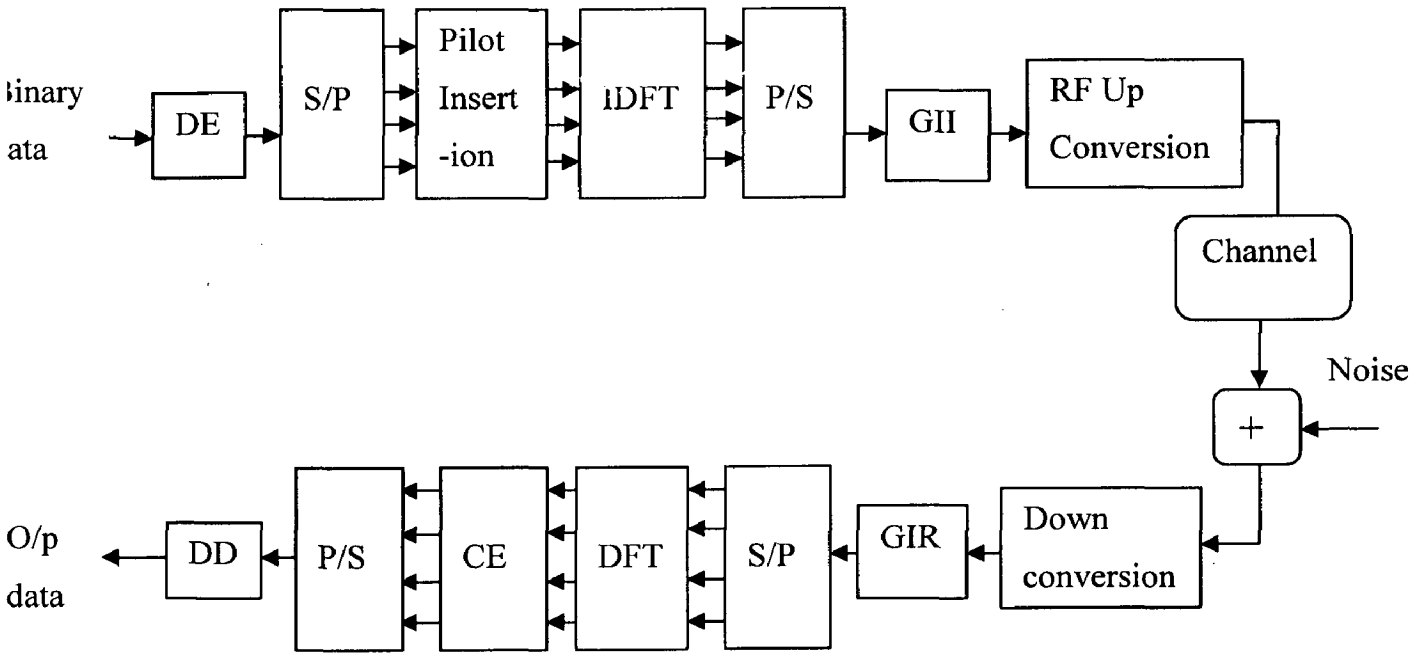

Figure 2.2 OFDM System Configuration

The k^{th} sample of the transmitted baseband OFDM signal can be expressed as

$$s(k) = \frac{1}{\sqrt{N}} \sum_{n=0}^{N-1} x(n) \exp\left(j2\pi kn / N \right) \qquad -N_g \le k \le N-1 \qquad (2.1)$$

where samples from $s(-N_g)$ to s(-1) denote the samples in the cyclic prefix of the symbol. N is the number of points in Inverse Fast Fourier Transform (IFFT), equivalent to the number of available sub-carriers, and $x(n)$ is the modulated data or sub-carrier symbol on n^{th} sub-carrier (which may assume any modulation like PSK or QAM). N_g denotes the number of samples in the cyclic prefix. Generally, not all the N sub-carriers carry data in an OFDM system. Most of the practical implementations of OFDM have a set of sub-carriers which are set to zero. These sub-carriers are called *Virtual Carriers*. These carriers are inserted to act as guard band from other systems working in the same frequency. These carriers may also be used for channel estimation purposes. Symbol energy can be given by the expression

$$E\left(|s(k)|^2\right) = \sigma_s^2 \tag{2.2}$$

sub-carrier spacing in such a system can be defined as $1/NT_s$ where T_s is the sample time. Consider a frequency selective multipath fading channel with average path gains (P_l : l = 0,1,...,L-1) (including possible paths with a zero gain) and the corresponding path delays τ_l such that $P_{L-1} \neq 0$. The value of N_g must be chosen so that $N_g \geq L$. Assuming that the path delays are sample-spaced, the equivalent channel impulse response of the channel can be written as

$$h(k) = \sum_{l=0}^{L-1} h_l \delta(k-l) \tag{2.3}$$

where

$$E\left(|h_l|^2\right) = P_l \qquad 0 \leq l \leq L-1 \tag{2.4}$$

at the receiver, there exist carrier- frequency offset and symbol-timing offset, which have to be estimated and compensated, assuming a perfect sampling clock. Thus, the k^{th} sample of the received symbol can be represented as

$$r(k) = \exp\left(j2\pi k\varepsilon / N\right) \sum_{l=0}^{L-1} h_l s(k-l-\theta) + n(k) \tag{2.5}$$

where *n(k)* is a sample of zero-mean complex Gaussian noise process with variance σ_n^2, ε is the carrier-frequency offset normalized with respect to the sub-carrier spacing and θ is the timing offset.

Number of Sub-Carriers

For a given symbol bandwidth (*BW*), the number of sub-carriers (*N*) should be chosen such that channel gain and phase can be considered approximately constant over each sub-carrier. If this criterion is not met, multi-tap equalization is required in each sub-band. This thesis does not consider such cases.

To achieve a nearly constant channel in each sub-band, the band width of each sub-band should be considerably smaller than the channel coherence bandwidth.

$$\frac{BW}{N} \ll CB$$

$$BW = \frac{1}{T_s}$$

$$N \gg \frac{1}{CB \times T_s} \tag{2.6}$$

where, $T_s = \frac{T}{N + N_g}$ is the sampling period, T is the time duration of one OFDM symbol after adding the guard interval. *CB,* the coherence bandwidth, is the frequency interval over which channel is correlated [3].

Length of the Guard Interval

Addition of the guard interval to the beginning of each OFDM symbol serves two purposes. First, if chosen sufficiently long, it prevents interference from previous OFDM symbols i.e., Inter-OFDM Symbol-Interference. The length of the guard interval should be chosen longer than the maximum expected channel delay

spread. Second, if chosen as the replica of the data points at the end of the OFDM symbol, it results in the simple multiplication relationship of the received sequence. Apart the above two, the insertion of CP can result in an equivalent parallel orthogonal channel structure that allows for simple channel estimation and equalization [11]. In spite of the loss of transmission power and bandwidth associated with the cyclic prefix. these properties generally motivate its use [5], [6].

2.2 Effect of Timing Offset

As mentioned earlier, symbol timing is aimed at detecting the start of the OFDM symbol. The detection becomes difficult when the channel experiences multipath fading. The cyclic prefix, on the other hand, alleviates some of the burden of symbol timing. An OFDM symbol is composed of cyclic prefix samples and useful data samples as shown in Figure 2.1, the cyclic prefix samples are inserted to overcome inter-symbol interference (ISI), whereas the useful samples are used for data recovery via the FFT [8]. For proper operation, the receiver should be able to determine the correct position of the FFT window. If the estimated symbol boundary falls within the cyclic prefix, it does not impair the performance, but a change in phase proportional to the subcarrier index will appear at the FFT output. Otherwise, the demodulated OFDM signal will be distorted by inter-symbol interference (ISI) and inter-carrier interference (ICI) [9], [17], i.e., When the beginning of the FFT window is placed outside the cyclic prefix sample, the signal to noise ratio (*SNR*) will also be reduced in addition to the phase change. Apart from the interference noise effect, timing offset affects channel estimation too [9]. Channel estimation is performed in a time-domain estimation window and the estimated channel impulse response (CIR) is required to be within this estimation window to produce an unbiased channel estimate. The timing offset shifts the location of the CIR along the time axis and degrades the channel estimation, once some portion of CIR is shifted outside the channel estimation window. The channel estimation performance affects the system performance directly, therefore, accurate timing is critical to good system performance [9]. Various symbol synchronization algorithms have been proposed in the literature [11], [14], [15], [18], [19]. Some algorithms require transmission of pilot symbols, whereas others are blind

2.3 Timing Error and Cyclic Prefix

2.3.1 OFDM Symbol Structure

The symbol structure of the discrete complex baseband OFDM signal is shown in Figure 2.3 [16].

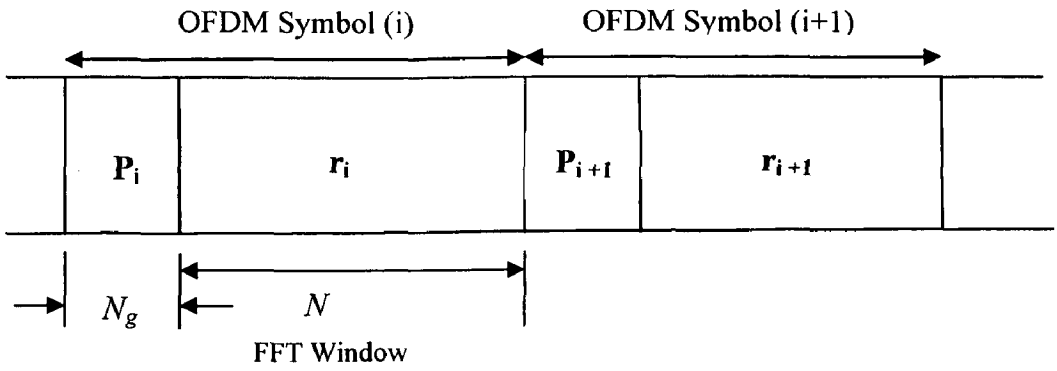

Figure 2.3 OFDM symbol structure

We denote N time domain complex samples (excluding CP) of the i^{th} OFDM symbol by $r_i(n),\ 0 \le n \le N-1$

$$\mathbf{r}_i = \left[r_i(0)\ \ r_i(1)\ \ .....\ \ r_i(N-1) \right] \tag{2.7}$$

The cyclic prefix of the i^{th} OFDM symbol, $\mathbf{p}_i$, consists of the last N_g samples of $\mathbf{r}_i$

$$\mathbf{p}_i = \left[r_i(N-N_g)\ \ .....\ \ r_i(N-1) \right] \tag{2.8}$$

The total i^{th} OFDM symbol (including CP) consists of the concatenation of vectors $\mathbf{p}_i$ and $\mathbf{r}_i$ with $N+N_g$ samples in length. Time synchronization task at the OFDM demodulator involves the determination of the starting sample of the i^{th} OFDM symbol such that CP (first N_g samples or $\mathbf{p}_i$) can be discarded and the next N samples can be aligned with the FFT window $\mathbf{w}_i$, such that

$$\mathbf{w}_i = \left[r_i(0)\ \ r_i(1)\ \ .....\ \ r_i(N-1) \right] \tag{2.9}$$

Therefore, the correctly (with no time synchronization error) demodulated data vector $\mathbf{R}_i$ corresponding to the i^{th} OFDM symbol is given by

$$\mathbf{R}_i = fft(\mathbf{w}_i) \tag{2.10}$$

where *fft*(.) denotes the fast Fourier transform operator. Misalignment in the FFT window can occur towards the CP or away from CP (into the next OFDM symbol), which results in erroneous demodulated data [16]. These two types of time synchronization error are discussed in the next following sections.

2.3.2 Timing Error towards CP

Figure 2.4 shows FFT window misalignment of the i^{th} OFDM symbol towards its own CP of d_i samples, the FFT window (erroneous) will capture d_i samples from its own CP and N-d_i samples from actual OFDM data, where $d_i \leq N_g$. Now we denote these two parts of the erroneous FFT window $\mathbf{w}_i^-$, by $\mathbf{u}_i^-$ and $\mathbf{v}_i^-$, respectively.

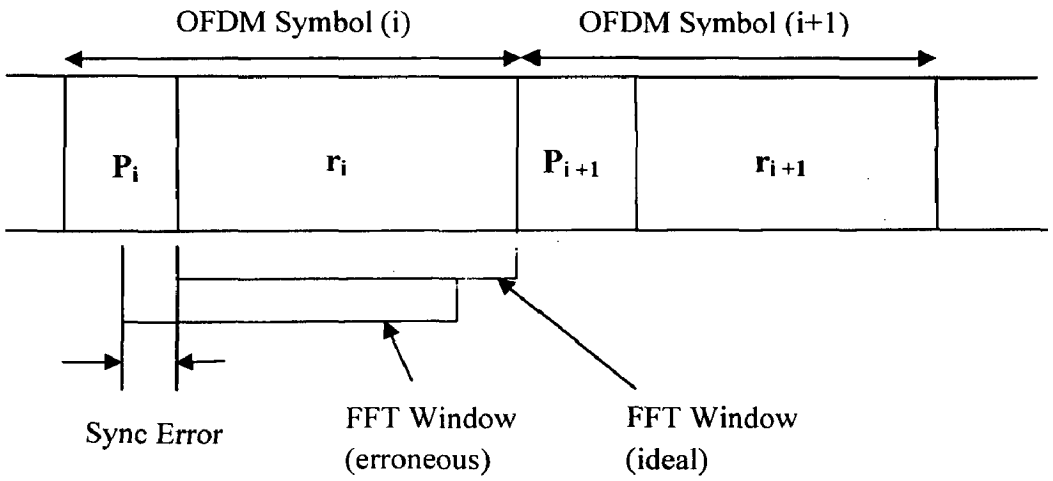

Figure 2.4 Symbol synchronization errors towards CP

Therefore,

$$\mathbf{w}_i^- = \begin{bmatrix} \mathbf{u}_i^- & \mathbf{v}_i^- \end{bmatrix} \tag{2.11}$$

where

$$\mathbf{u_i}^{-} = \left[r_i(N-d_i) \;\; r_i(N-d_i+1) \;\; .....r_i(N-1) \right]$$

$$\mathbf{v_i}^{-} = \left[r_i(0) \;\; r_i(1) \;\; ..... \;\; r_i(N-d_i-1) \right]$$

and the demodulated data for the i^{th} OFDM symbol becomes

$$\mathbf{R_i}^{-} = fft\left(\mathbf{w_i}^{-}\right) \tag{2.12}$$

using the circular shift property of the FFT it can be shown that

$$R_i^{-}(k) = R_i(k)\exp\left(-j\frac{2\pi}{N}kd_i\right) \quad for \quad k = 0,1,2,.....N-1 \tag{2.13}$$

where, $R_i^{-}(k)$ and $R_i(k)$ are the k^{th} element of the vectors $\mathbf{R_i}^{-}$ and $\mathbf{R_i}$, respectively. $\mathbf{R_i}$ is the correctly demodulated i.e., with zero time synchronization error, data for the i^{th} OFDM symbol as given in equation (2.10). If a perfect channel with no noise or fading is assumed, each $R_i(k)$ should correspond to some constellation point. For an example, in the case of QPSK they come from the constellation $1\angle 45^{\circ}$, $1\angle -45^{\circ}$, $1\angle 135^{\circ}$, and $1\angle -135^{\circ}$. According to equation (2.13), for a timing error of d_i samples towards the CP the data carried by the k^{th} sub-carrier experiences a phase shift of $-\frac{2\pi}{N}kd_i$. This is the case for coherent (non-differential) modulation. Even for a small window misalignment (e.g. d_i=1), the OFDM subcarriers at the high frequency end (large k) experience large phase shifts causing data to map into incorrect constellation points. This results in severe degradation in BER performance. However, if differential modulation is employed across the subcarriers of the same OFDM symbol, the detrimental effect of the time synchronization error can be greatly reduced. This is due to the fact that adjacent subcarriers in the differential case experience a constant phase shift of $-\frac{2\pi}{N}d_i$ irrespective of subcarrier position (index k) within the OFDM symbol. Therefore, only large synchronization error (d_i) can cause mapping errors [16] [17].

2.3.3 Timing Error away from CP

Figure 2.5 shows a case of FFT window misalignment of the i^{th} OFDM symbol away from the CP i.e., in to the next (i+1th) OFDM symbol

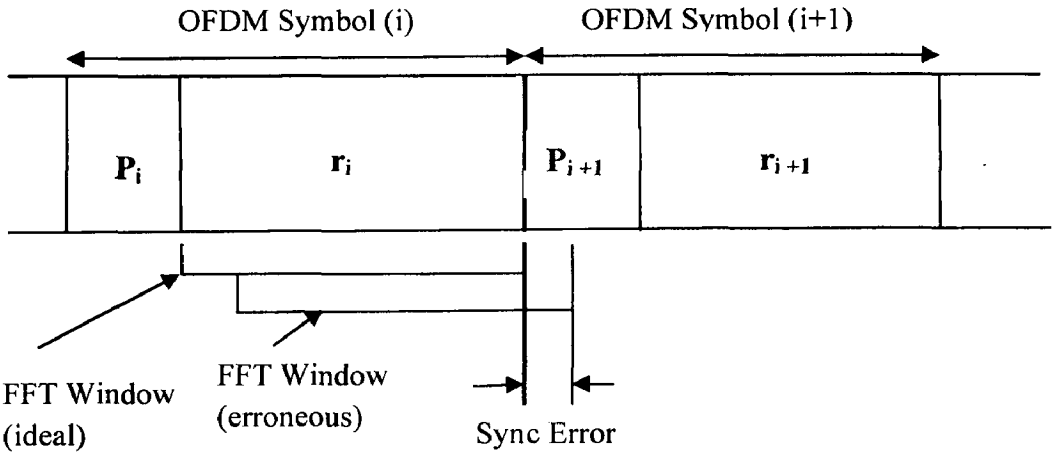

Figure 2.5 Symbol synchronization errors away from CP

If the synchronization error is d_i samples, the erroneous FFT window $\mathbf{w}_i^+$ captures (N-d_i) samples from the i^{th} OFDM symbol, and d_i samples from the CP of the (i+1)th OFDM symbol. Therefore,

$$\mathbf{w}_i^+ = \left[\mathbf{u}_i^+ \quad \mathbf{v}_i^+\right] \tag{2.14}$$

where,

$$\mathbf{u}_i^+ = \left[r_i(d_i) \quad r_i(d_i+1) \quad \ldots\ldots \quad r_i(N-1)\right]$$

$$\mathbf{v}_i^+ = \left[r_{i+1}(N-N_g) \quad \ldots\ldots \quad r_{i+1}(N-N_g+d-1)\right]$$

The demodulated data for the i^{th} OFDM symbol becomes

$$\mathbf{R}_i^+ = fft\left(\mathbf{w}_i^+\right) \tag{2.15}$$

from (2.14) and (2.15) $R_i^+(k)$ can be proved as [16]

$$R_i^+(k)$$

$$= \sum_{n=0}^{N-d_i-1} r_i(n+d_i)\exp\left(-j\frac{2\pi}{N}kn\right)+\sum_{n=N-d_i}^{N-1} r_{i+1}(n+d_i-N_g)\exp\left(-j\frac{2\pi}{N}kn\right)$$

$$= \sum_{m=d_i}^{N-1} r_i(m)\exp\left(-j\frac{2\pi}{N}k(m-d_i)\right)+\sum_{m=0}^{d_i-1} r_{i+1}(m+N-N_g)\exp\left(-j\frac{2\pi}{N}k(m-d_i)\right)$$

$$= \sum_{m=0}^{N-1} r_i(m)\exp\left(-j\frac{2\pi}{N}k(m-d_i)\right)-\sum_{m=0}^{d_i-1} r_i(m)\exp\left(-j\frac{2\pi}{N}k(m-d_i)\right)+$$

$$\sum_{m=0}^{d_i-1} r_{i+1}(m+N-N_g)\exp\left(-j\frac{2\pi}{N}k(m-d_i)\right)$$

$$=\left[R_i(k)+ISI_i(k)\right]\exp\left(j\frac{2\pi}{N}kd_i\right). \qquad (2.16)$$

where,

$$ISI_i(k)=\sum_{m=0}^{d_i-1}\left[r_{i+1}(m+N-N_g)-r_i(m)\right]\exp\left(-j\frac{2\pi}{N}km\right).$$

According to (2.16), the data carried by the k^{th} subcarrier of the i^{th} OFDM symbol, $R_i(k)$, experience an inter-symbol-interference (ISI) term of $ISI_i(k)$, and a phase rotation of $\frac{2\pi}{N}kd_i$. The influence of the ISI term can be more detrimental to the BER performance of the OFDM system. The effect of the phase shift term $\frac{2\pi}{N}kd_i$ can be significantly reduced by employing differential modulation as in the case described in the previous section. It should be noted that the introduction of the ISI term can be avoided by incorporating a short cyclic postfix at the end of each OFDM symbol. But this would be waste of power and system *BW*, and therefore, is not typically used. Cyclic prefix on the other hand is preliminarily incorporated to mitigate the multipath problem by making the CP longer than the channel memory [16].

2.4 Existing Techniques for Timing Synchronization

Timing synchronization is usually divided into a coarse timing phase and a fine timing phase. Different systems would have different requirements for symbol timing. For example, WLANs can only use the preambles whereas broadcast systems can employ many symbols to gradually acquire more accurate symbol timing [8] [20].

2.4.1 Coarse Timing

Coarse timing is usually the first task performed in the OFDM synchronization procedure. During the timing acquisition phase, it has to be assumed (in practice) that the carrier frequency offset is completely unknown. Hence the orthogonality of the subcarriers may not be retained to provide a useful post-FFT signal. Consequently, coarse timing is employed in time domain.

Depending on different system requirements, the coarse timing can be carried out by utilizing either the OFDM inherent cyclic prefix [10], [11], [17] [21] or the specially designed training sequence (preamble) [13], [14], [22]. By utilizing the cyclic prefix, the algorithms can work 'blindly' without the overhead of a known training sequence, whereas employment of a training sequence can usually result in a faster and more robust synchronization. For both the cyclic prefix and the training-sequence-based schemes, there are basically three methods for coarse timing, i.e., the maximum likelihood (ML) [11], minimum mean squared error (MMSE) [17], [18] and the maximum correlation (MC) [10] methods.

2.4.2 Fine Timing

Fine timing is usually the last step in the timing acquisition process. Fine timing can be achieved through correlation either in the time domain [15], [23] or in the frequency domain [7], [10], [24]. Frequency-domain based schemes first estimate the channel impulse response after the FFT, then fine-tune the position of the estimated channel impulse response (CIR) with respect to the FFT-window. Because the frequency-domain based schemes can effectively resolve channel multi-

paths, they generally render better performance than the time-domain schemes in multipath fading channels. For the frequency-domain based schemes, there are different approaches to tracking the estimated CIR in the FFT-window. One method is to locate the peak position of the estimated CIR. There are many modified peak-finding versions when the noise effect is considered and when the first peak is not the largest peak in the CIR.

Chapter 3

SYMBOL TIME OFFSET ESTIMATION ALGORITHMS FOR OFDM

OFDM is used in both broadcast networks, like Digital Audio Broadcasting (DAB) and Digital Video Broadcasting (DVB), and in packet switched environment, like WLANs [6] [25]. While the broadcast systems can initially spend a relatively long time to acquire the signal, packet switched networks usually require the synchronization to be required during a very short time after the start of the packet. Further, to achieve high system throughput, the receiver overhead must be kept to a minimum.

To facilitate the single-shot synchronization, current WLAN standards include a preamble, like the IEEE 802.11a [25] preamble shown in Figure 3.1 or the various HiperLAN/2 preambles, in the start of the packet. The length and the contents of such preamble sequences are carefully designed to provide enough information for good synchronization performance without any unnecessary overhead. For example, in Figure 3.1, The IEEE 802.11a standard gives guidelines on how to use the various segments of the preamble to perform the necessary synchronization functions. A_1 to A_{10} are called short training sequences or short codes, which are identical and 16 samples long. They are used for packet detection; frequency offset estimation and symbol timing. C_1 and C_2 are long training sequence, identical and 64 samples long. They are used for channel estimation; frequency offset estimation and symbol timing estimation. However, the guidelines are not binding requirements of the standard.

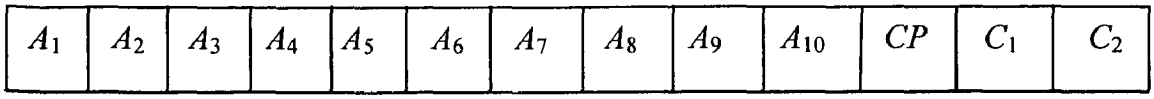

Figure 3.1 The IEEE 802.11a preamble

Besides the preamble based synchronization techniques, we also have several non-data aided estimation techniques. Such techniques either use the innate

redundancy provided in the structure of OFDM symbol by the cyclic prefix or utilize some higher order statistics for correct estimation, and also a time offset estimator that exploits both the redundancy introduced by the cyclic prefix and the channel estimation pilots. In this chapter, a short overview of various synchronization techniques, for symbol timing estimation, available in literature is provided. Both cyclic prefix based and the pilot signals in conjunction with the redundancy present in the cyclic prefix.

3.1 Symbol Time Offset Estimation Techniques

There are several algorithms available in literature for timing estimation. Some of them utilize the properties of specific pilots or preamble sequences [14], [22], [26] for attaining proper synchronization. Such algorithms are generally termed as data aided algorithms. Besides the data aided schemes, there are non- data aided or blind schemes which do not use any preamble or pilot sequences [11], [27], [28] for estimation. Most of these non-data aided schemes utilize the inherent redundancy available in OFDM symbols, in the form of cyclic prefix, for estimation. Some of the data aided algorithms, which don't require the knowledge of the exact preamble sequences transmitted, are sometimes also referred to as blind estimators. Besides these there are hybrid schemes, in which both the redundancy in the cyclic prefix and the pilot symbols are exploited for efficient symbol time offset estimation [15]. [23]. We discuss various preamble based, cyclic prefix based and both cyclic prefix and pilot based timing offset estimation algorithms in this section.

As explained in the previous sections, timing estimation essentially consists of two main sub tasks: coarse timing estimation or packet synchronization, where we try to achieve a rough estimate of the start of the incoming packet, and symbol synchronization or fine timing, where we refine the rough estimate to obtain the actual DFT window.

3.1.1 Preamble Based Synchronization Techniques

Schmidl and Cox's Algorithm

Packet detection algorithms utilize some repetitiveness in the preamble symbols. The groundwork for most of these algorithms is done by Schmidl and Cox

(S&C) in [14]. The algorithm can be used for both timing and frequency synchronization. Further, the results from packet detection algorithm can directly be used to find the actual DFT window i.e., there's no requirement of a separate symbol timing estimation algorithm.

In their algorithm, timing recovery relies on searching for a training symbol with two identical halves in the time domain, which would remain identical after passing through the channel, except that there will be a phase difference between them caused by the carrier frequency offset. The two halves of the training symbol are made identical (in time domain) by transmitting a PN sequence on the even frequencies, while zeros are transmitted on the odd frequencies, to form the first training symbol (Short Code). The second training symbol (Long Code) contains a PN sequence on the odd frequencies to measure these sub-carriers, and another PN sequence on the even frequencies to help determine frequency offset. The PN sequence can be appropriately chosen depending on the desired properties like peak-to-average power ratio, high correlation etc. The preamble structure is shown in Figure 3.2. The timing metric is computed using the correlation of symbols in two length N/2 windows. The resultant value is divided by the total energy of the symbols present in the second window to obtain a normalized metric.

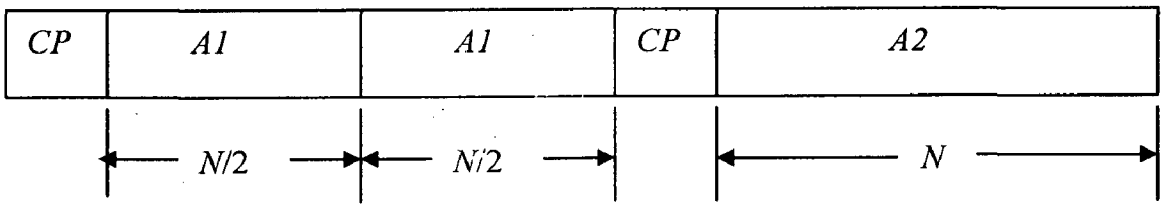

Figure 3.2 Preamble for Schmidl and Cox's Algorithm

Then the Schmidl and Cox's timing estimator takes as the start of the symbol the maximum point of the timing metric given by

$$M(d) = \frac{|P(d)|^2}{R^2(d)} \tag{3.1}$$

where $d = \theta$ is a time index corresponding to the first sample in a window of N samples and

$$p(d) = \sum_{m=0}^{\frac{N}{2}-1} \left(r^*(d+m).r\left(d+m+\frac{N}{2}\right)\right) \tag{3.2}$$

and

$$R(d) = \sum_{m=0}^{\frac{N}{2}-1} \left| r\left(d+m+\frac{N}{2}\right)\right|^2 \tag{3.3}$$

The timing metric reaches a plateau with length equal to the length of the guard interval minus the length of the channel impulse response, as there would be no ISI within this plateau to distort the signal. For the AWGN channel, this plateau is of the length of the guard interval, and the start of the frame can be taken to be anywhere within this window without a loss in the received SNR. For the frequency selective channels, the length of the impulse response of the channel is shorter than the guard interval by design choice of the guard interval, so the plateau in the maximum of the timing metric is shorter than for the AWGN channel.

The timing metric reaches a plateau, which leads to some uncertainty as to the start of the frame. To alleviate this, Schmidl and Cox proposes an averaging method where the maximum point is first found and then two points with 90% of the maximum value, one to the left and the other to the right of the maximum point, are found. The timing estimate is taken as the average of the two 90% points [14].

Variants of Schmidl and Cox's Algorithm

Various other timing estimation algorithms proposed in the literature are generally variants of the S&C algorithm. In [14], the authors try to overcome the uncertainty due to the timing metric plateau and thus improve the timing offset estimation scheme proposed by Schimdl and Cox.

A. Sliding Window Method

Firstly, in calculation of the half symbol energy $R(d)$ in equation (3.3), all samples over one symbol period (excluding guard interval) is used instead of over the second half symbol period.

Secondly, instead of 90% points averaging approach, the timing metric is simply averaged over a window of length $N_g + 1$ samples. Then the timing metric is given by

$$M_1(d) = \frac{1}{N_g + 1} \sum_{k=-N_g}^{0} M_f(d+k) \tag{3.4}$$

where $M_f(d)$ can be calculated as

$$M_f(d) = \frac{|P(d)|^2}{R_f^2(d)} \tag{3.5}$$

and

$$R_f(d) = \frac{1}{2} \sum_{m=0}^{N-1} |r(d+m)|^2$$

and $p(d)$ is given by equation (3.2).

B. Training Symbol Method

The samples of the training symbols (excluding cyclic prefix) are designed to be of the form

$$s = [A\ A\ -A\ -A] \tag{3.6}$$

where A represents samples of length $l=N/4$ generated by $N/4$ point IFFT of $N_u/4$ length modulated data of a PN sequence. The abrupt amplitude change due to sign conversion in the training symbol can easily be avoided by modifying the PN sequence such that the sum of the corresponding modulated data equals to zero. Then the timing metric is given by

$$\mathrm{M}_2(d) = \frac{|P_2(d)|^2}{R_2^2(d)} \tag{3.7}$$

where

$$P_2(d)=\sum_{k=0}^{1}\sum_{m=0}^{l-1} r^*(d+2lk+m).r(d+2lk+m+l) \tag{3.8}$$

and

$$R_2(d)=\sum_{k=0}^{1}\sum_{m=0}^{l-1}\left|r(d+2lk+m+l)\right|^2 \tag{3.9}$$

In both methods, $P_2(d)$ and $R_2(d)$ or $P(d)$ and $R_f(d)$ can be calculated iteratively. The correct timing point is taken as the start of the useful part of training symbol (after cyclic prefix).

3.1.2 Cyclic Prefix Based ML Estimator

As stated earlier, Non-data aided schemes generally utilize the redundancy introduced by the cyclic prefix in the OFDM system. We present and evaluate the joint maximum likelihood (ML) estimation of the time and carrier-frequency offset in OFDM systems. The key element that will rule the discussion is that the OFDM data symbols already contain sufficient information to perform synchronization [11]. The ML algorithm exploits the cyclic prefix preceding the OFDM symbols, thus reducing the need for pilots. Because of the two uncertainties in the receiver of OFDM system and the AWGN thus yield the received signal

$$r(k)=s(k-\theta)\exp\left(j2\pi\varepsilon k/N\right)+n(k) \tag{3.10}$$

where, the first term in the right side of the equation (3.10) is the transmitted signal with integer-valued unknown arrival time (θ) of a symbol and frequency offset ε. Authors in [11] obtain an estimator assuming that the transmitted symbols are uncorrelated. It assumes the observation of $2N+N_g$ samples with one complete OFDM symbol of length ($N+N_g$) present within as shown in Figure 3.3. The position of this symbol within the observed block of samples, however, is unknown because the channel delay θ is unknown to the receiver.

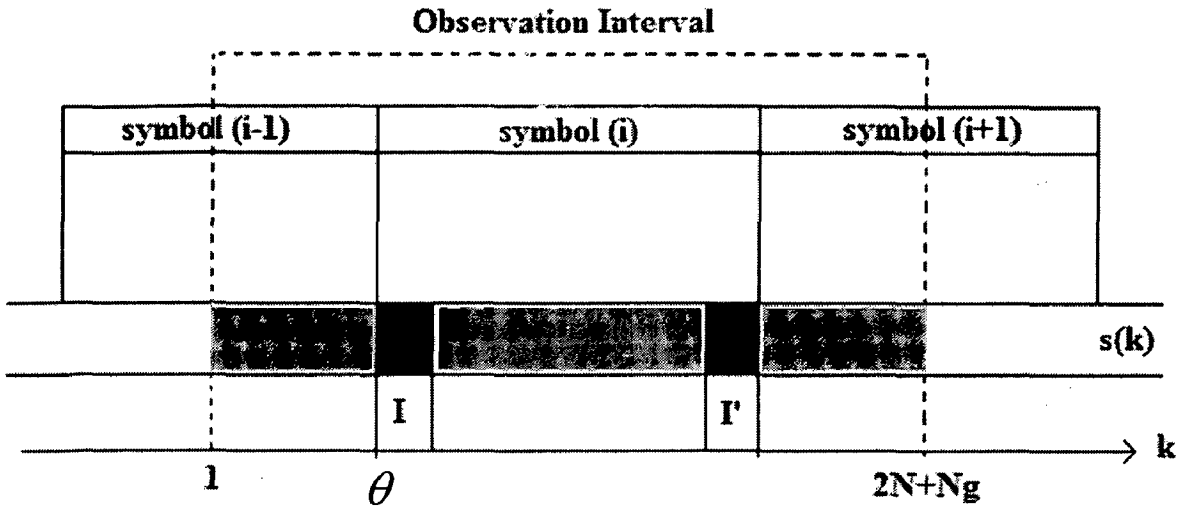

Figure 3.3 Structure of OFDM signal with cyclically extended symbols *s(k)*

Define the index sets

$I \triangleq \{\theta,....,\theta+N_g-1\}$ and

$I' \triangleq \{\theta+N,...,\theta+N+N_g-1\}$

The set I' thus contains the indices of the data samples that are copied into the cyclic prefix, and the set I contains indices of this prefix. The observed samples in the $(2N+N_g)\times 1$-vector i.e.,

$\boldsymbol{r} \triangleq [\mathrm{r}(1).....\mathrm{r}(2N+N_g)]^T$

Notice that the samples in the cyclic prefix and their copies are pair wise correlated, while the remaining samples are mutually uncorrelated. The estimator can be described using the equations (3.11), (3.12) and (3.13). As can be observed, it is essentially a joint estimation algorithm where both symbol timing offset and frequency offset are jointly estimated, shown in Appendix A.

$$\Lambda(\theta,\varepsilon)=|\gamma(\theta)|\cos(2\pi\varepsilon+\angle\gamma(\theta))-\rho\Phi(\theta) \qquad (3.11)$$

where $\angle$ denotes the argument of a complex number.

$$\gamma(\theta)=\sum_{k=\theta}^{\theta+N_g-1} r(k)r^*(k+N) \tag{3.12}$$

$$\Phi(\theta)=\frac{1}{2}\sum_{k=\theta}^{\theta+N_g-1} |r(k)|^2+|r(k+N)|^2 \tag{3.13}$$

and

$$\rho=\frac{SNR}{SNR+1} \tag{3.14}$$

where

$SNR=\sigma_s^2/\sigma_n^2$, $\sigma_s^2 \triangleq E\{|s(k)|^2\}$ and $\sigma_n^2 \triangleq E\{|n(k)|^2\}$.

ρ is the magnitude of the correlation coefficient between $r(k)$ and $r(k+N)$. $\Phi(\theta)$ is an energy term, independent of the frequency offset. The maximization of the log-likelihood function can be performed in two steps. Initially we could obtain the maximum with respect to ε, and then maximize the likelihood function with respect to timing offset using the value of frequency offset obtained. The maximum with respect to the frequency offset ε is obtained when the cosine term in equation (3.11) equals to one. This results in

$$\hat{\varepsilon}_{ML}(\theta)=-\frac{1}{2\pi}\angle\gamma(\theta)+n \tag{3.15}$$

where n is an integer, which accounts for the fact that several maxima exist for a cosine function. $n=0$ if it can be assumed that $|\varepsilon|\leq 1/2$. In such a case, the ML estimates become

$$\hat{\theta}_{ML}=\arg\max_{\theta}\{|\gamma(\theta)|-\rho\Phi(\theta)\} \tag{3.16}$$

$$\hat{\varepsilon}_{ML} = -\frac{1}{2\pi}\angle\gamma(\hat{\theta}_{ML}) \tag{3.17}$$

Only two quantities affect the log likelihood function. the number of samples in the cyclic prefix N_g, and the correlation coefficient ρ given by the *SNR*. If ε is a priori known to be zero, the log-likelihood function for θ becomes

$$\Lambda(\theta) = \mathrm{Re}\{\gamma(\theta)\} - \rho\Phi(\theta) \tag{3.18}$$

and $\hat{\theta}_{ML}$ is its maximizing argument. The equations (3.16) and (3.17) describe an open-loop structure. Closed-loop implementation may also be considered. In such structures, the signal $\Lambda(\theta, \hat{\varepsilon}_{ML}(\theta))$ is typically fed back in a phase-locked loop (PLL). If we can assume that θ is constant over a certain period, the integration in the PLL can significantly improve the performance of the estimators [11], [26].

3.1.3 Hybrid ML Estimation Using both CP and the Pilot Symbols

In practice, most coherent OFDM systems transmit pilot symbols on some of the sub-carriers to estimate channel attenuation and also add a cyclic prefix (CP) to avoid inter-carrier interference and inter-symbol interference. In this section, hybrid maximum-likelihood estimation algorithm based on the redundancy of both cyclic prefix and pilot sub-carriers is presented for the symbol time offset estimation. In coherent OFDM systems, the symbol transmission through the channel is accomplished in the time-domain. The symbol time offset in the time-domain induces the phase change in the received symbols in the frequency-domain, increasing symbol error rate eventually. The symbol time offset estimation method using the pilot signals in conjunction with the redundancy present in the cyclic prefix was proposed in [15], where evenly spaced pilot signals were used to enhance the accuracy of the symbol time offset estimator in addition to redundancy present in the cyclic prefix [11], [12]. But the contribution of pilot signal is lowered by their evenly spaced positions within on OFDM symbol and also by using the same pilot signal sets for all OFDM symbols. Because evenly spaced pilot signals in the frequency-domain have large correlation in the time domain, the ML function of the

symbol time offset estimator may attain its maximum value at an inaccurate value of time offset. As a result, the variance of estimate increases and the performance of the estimator is degraded. Therefore the authors in [23] presented the pilot signal design algorithms with a purpose that the pilot signals have low correlation in the time-domain. These algorithms are developed in terms of positions and value of pilot signals in order to enhance the accuracy of the symbol time offset estimator.

The Signal Model

Both the cyclic prefix and the pilots contain information about the symbol start, which can be exploited. One transmitted OFDM symbol consists of N subcarriers of which N_p are modulated by pilot symbols. Let P denote the set of indexes of the N_p pilot carriers. We separate the transmitted signal in two parts. The first part contains the $N - N_p$ data subcarriers and is modelled by

$$s(k) = \frac{1}{\sqrt{N}} \sum_{n \in \{0,\ldots N-1\} \setminus P} x(n) e^{j2\pi kn/N} \tag{3.19}$$

where $x(n)$ is the data symbol transmitted on the nth subcarrier, under a certain fixed constellation with an average energy $\sigma_x^2 = E\{|x(n)|^2\}$. The second part contains the N_p pilot subcarriers, modelled by

$$m(k) = \frac{1}{\sqrt{N}} \sum_{n \in P} p(n) e^{j2\pi kn/N} \tag{3.20}$$

where $p(n)$ is the pilot symbol transmitted on the nth subcarrier, and assume.

$$E\{|p(n)|^2\} = \sigma_x^2$$

Now for the AWGN channel the received signal *r(k)* is represented by the following equation.

$$r(k) = s(k-\theta) + m(k-\theta) + n(k) \tag{3.21}$$

The value θ can be estimated using two properties of the received signal *r(k);* the statistical properties of the time-domain data signal *s (k),* and the knowledge of the time-domain pilot signal, *m(k).*

In the model [23], they assumed that the transmitted signal *s(k)* is a Gaussian process with variance $\alpha\sigma_x^2$, where $\alpha = \frac{N - N_p}{N}$. Since the noise is zero-mean Gaussian and the pilot signal *m(k)* is a deterministic signal which is known at the receiver, the modelled received signal *r(k)* is also Gaussian with time-varying mean *m(k)* and variance $\alpha\sigma_x^2$. Collect the observed samples in the $(2N+N_g)\times 1$-vector with one complete OFDM symbol within. Based in the model (3.21), we derive the ML estimator of the time offset θ by investigating the log-likelihood function of θ, i.e., the joint probability of the received samples *r*(.) given θ,

$$\Lambda(\theta) = \log \Pr[\mathbf{r}(.) = \mathbf{r}(.) \mid \theta] \tag{3.22}$$

where $\Pr[.]$ denotes the probability density function of the variables in its argument. The ML estimate θ is acquired by maximizing this log-likelihood function over all possible values of θ as the following equation:

$$\hat{\theta}_{ML} = \arg\max_{\theta}\{\Lambda(\theta)\} \tag{3.23}$$

The estimator can be described using the equations (3.24), (3.25) and (3.26). In Appendix B, $\Lambda(\theta)$ is shown to be

$$\Lambda(\theta) = \rho\Lambda_{cp}(\theta) + (1-\rho)\Lambda_p(\theta) \tag{3.24}$$

where

$$\Lambda_{cp}(\theta) = \mathrm{Re}\left\{\sum_{k=\theta}^{\theta+N_g-1} r^*(k)r(k+N)\right\} - \frac{\rho}{2}\sum_{k=\theta}^{\theta+N_g-1}\left\{|r(k)|^2 + |r(k+N)|^2\right\} \tag{3.25}$$

exploits the information contained in the redundancy due to the cyclic prefix in the received signal and

$$\Lambda_p(\theta) = (1+\rho)\,\mathrm{Re}\left\{\sum_k r^*(k)m(k-\theta)\right\} - \rho\,\mathrm{Re}\left\{\sum_{k=\theta}^{\theta+N_g-1}(r(k)+r(k+N))^* m(k-\theta)\right\} \tag{3.26}$$

exploits the information contained in the pilot symbols with correlation coefficient

$$\rho = \frac{\alpha\sigma_x^2}{\alpha\sigma_x^2+\sigma_n^2} = \frac{\alpha SNR}{\alpha SNR+1} \tag{3.27}$$

Note how the contributions $\Lambda_{cp}(\theta)$ and $\Lambda_p(\theta)$ support each other. The contribution from the cyclic prefix gives an unambiguous but coarse estimate. The contribution from the pilots has very distinct peaks, but would by itself yield an unacceptable ambiguity. The evenly spaced pilots result in many correlation peaks. Together, however, they properly weighted contributions yield an unambiguous and distinct peak in the log-likelihood function. The peaks of $\Lambda_p(\theta)$ fine-tune the coarse estimate based on $\Lambda_{cp}(\theta)$. For a large *SNR* ($\rho \approx 1$), the estimate is mainly based on the cyclic prefix redundancy, whereas for a low *SNR* ($\rho \approx 0$) the estimate relies more on the pilot symbols [23].

Pilot Signal Design Algorithms

Motivation

First, we present the factor that gives rise to error in the estimator of (3.24). i.e., substitute (3.21) for the term *r(k)* in (3.26), and θ_t denotes the true time offset, each term of (3.26) is separated as follows:

$$r^*(k)m(k-\theta) = s^*(k-\theta_t)m(k-\theta) + m^*(k-\theta_t)m(k-\theta) + n^*(k)m(k-\theta) \tag{3.28}$$

$$\left(r(k)+r(k+N)\right)^* m(k-\theta)$$

$$=\left\{s^*(k-\theta_t)m(k-\theta)+m^*(k-\theta_t)m(k-\theta)+n^*(k)m(k-\theta)\right\}$$

$$+\left\{s^*(k+N-\theta_t)m(k-\theta)+m^*(k+N-\theta_t)m(k-\theta)+n^*(k+N)m(k-\theta)\right\} \quad (3.29)$$

Therefore, (3.26) can be written as

$$\Lambda_p(\theta)=(1+\rho)\mathrm{Re}\left\{\sum_k s^*(k-\theta_t)m(k-\theta)+\sum_k m^*(k-\theta_t)m(k-\theta)+\sum_k n^*(k)m(k-\theta)\right\}$$

$$-\rho\,\mathrm{Re}\sum_{k\in I}\begin{Bmatrix} s^*(k-\theta_t)m(k-\theta)+m^*(k-\theta_t)m(k-\theta) \\ +n^*(k)m(k-\theta)+s^*(k+N-\theta_t)m(k-\theta) \\ +m^*(k+N-\theta_t)m(k-\theta)+n^*(k+N)m(k-\theta)\end{Bmatrix} \quad (3.30)$$

Since, *s(k)* is assumed to be a Gaussian process with variance $\alpha\sigma_x^2$, *m(k)* is assumed to be a deterministic signal known to the receiver, and *n(k)* is assumed to be an additive complex white zero-mean Gaussian receiver noise. Therefore the magnitude of the following six terms depending on *s(k)* and *n(k)* cannot be controlled:

$$\sum_k s^*(k-\theta_t)m(k-\theta),\quad \sum_k n^*(k)m(k-\theta),\quad \sum_{k\in I} s^*(k-\theta_t)m(k-\theta),$$

$$\sum_{k\in I} n^*(k)m(k-\theta),\quad \sum_{k\in I} s^*(k+N-\theta_t)m(k-\theta),\ \text{and}\ \sum_{k\in I} n^*(k+N)m(k-\theta)$$

Thus, if we disregard these terms, (3.26) can be approximated as follows:

$$\Lambda_p(\theta)\approx(1+\rho)\mathrm{Re}\sum_k m^*(k-\theta_t)m(k-\theta)$$

$$-\rho\,\mathrm{Re}\sum_{k\in I}\left\{m^*(k-\theta_t)m(k-\theta)+m^*(k+N-\theta_t)m(k-\theta)\right\}. \quad (3.31)$$

in (3.31), the first term can mainly contribute to increase of $\Lambda_p(\theta)$ and now let us investigate how the periodicity of *m(k)* may affect the magnitude of $\Lambda_p(\theta)$. If *m(k)* is a periodic signal with a period *T*, i.e. *m(k)=m(k-T)*, $\forall k$ then $m^*(k-\theta_t)m(k-\theta)$

is equal to $m^*(k-\theta_t)m(k-(\theta+T))$. Therefore $\Lambda_p(\theta)$ will become large at points, θ_t, θ_t+T, θ_t+2T, etc., resulting in multiple peaks in log-likelihood function, $\Lambda_p(\theta)$. To confirm this statement, we show the contribution of the functions $\Lambda_{cp}(\theta)$, $\Lambda_p(\theta)$, and log-likelihood function $\Lambda(\theta)$ in Figure 3.4.

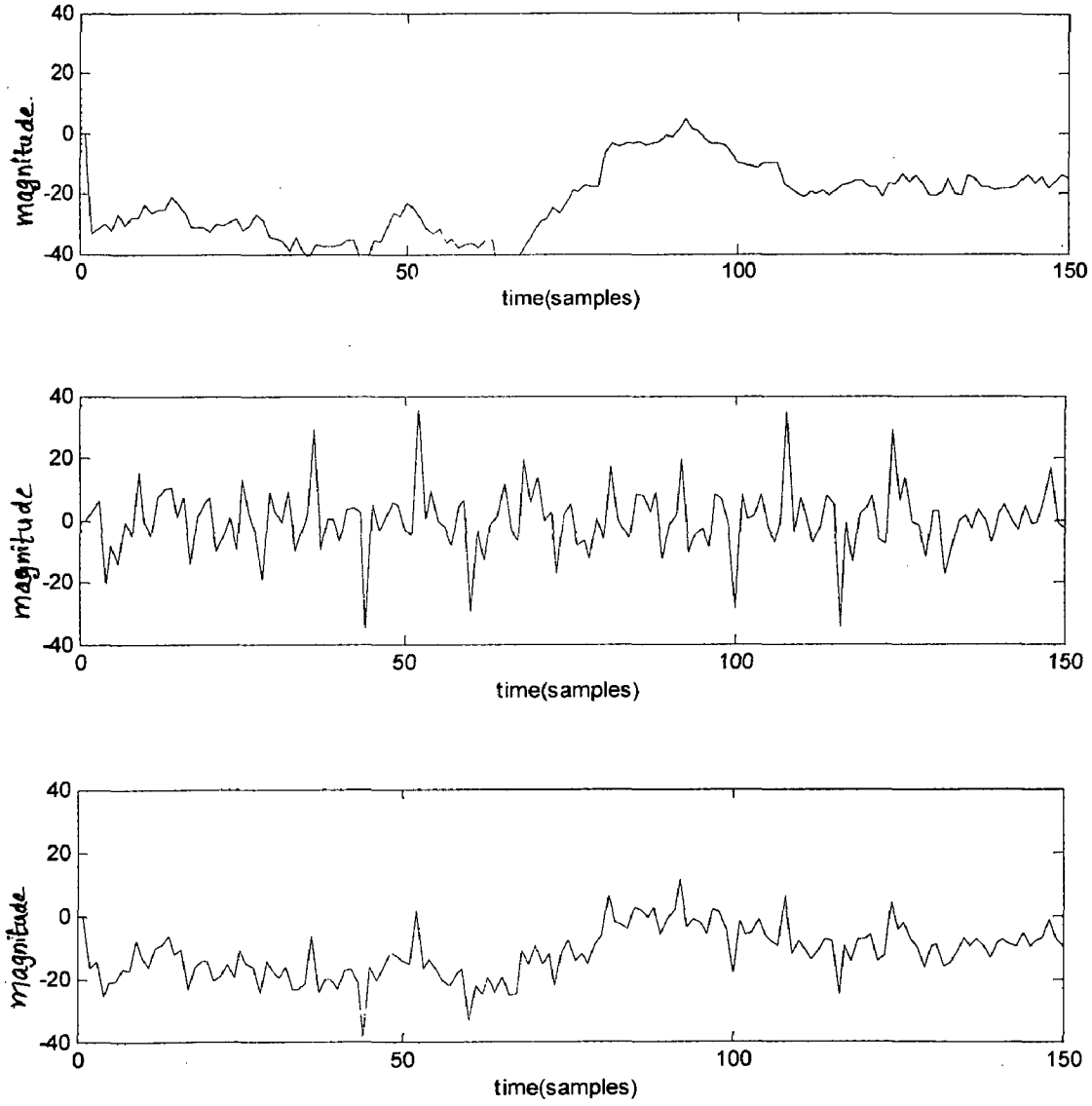

Figure 3.4 The ML estimator statistics in the AWGN channel with evenly spaced pilot signals. Contribution of redundancy of cyclic prefix (top), contribution of pilot signal (middle) resulting log-likelihood function (bottom), one OFDM symbol is $(N+N_g)$=144 samples and *SNR* is 1dB.

Figure 3.4 shows that $\Lambda_p(\theta)$ has many peaks at the other values of θ as well as at the true time offset value, θ_t. Hence, the estimation results may become ambiguous. In spite of this disadvantage for symbol time offset estimation, evenly spaced pilot signal shows the best performance for channel estimation, which is the original purpose of pilot signals. Through the investigations, we are to design the (frequency-domain) pilot signal so that the (time-domain) pilot signal can have lower periodicity than perfectly-equally spaced pilot signal [23].

The Requirements in the Pilot Signal Design

(i) The values of the frequency-domain pilot signals should belong to a certain fixed constellation. Therefore, if the set of the possible values in a fixed constellation is $A_M = \{a_0, a_1, a_2, ..., a_{M-1}\}$, then $p(n) \in A_M$.

(ii) The periodicity of the (time-domain) pilot signal m(k) should be lowered.

(iii) The power of the pilot symbol is equal to that of the data symbol, i.e. $E\{|p(n)|^2\} = E\{|x(n)|^2\} = \sigma_x^2$.

Pilot Signal Design Algorithm: Sine

As we can see in Figure (3.4), the sum of contribution of $\Lambda_{cp}(\theta)$ and $\Lambda_p(\theta)$ is the overall log-likelihood function $\Lambda(\theta)$. $\Lambda_{cp}(\theta)$ has unambiguous but coarse maximum value at a true time offset point, and has small values at distant points from a true time offset. Therefore, at a distant point from a true time offset, even if $\Lambda_p(\theta)$ has a large value (peak), $\Lambda(\theta)$ does not become very large because the contribution of $\Lambda_{cp}(\theta)$ is small. Therefore, *p(n)* can be chosen such that the (time-domain) pilot signal *m(k)* becomes similar to low-frequency sine wave. For example, for the QPSK constellation, $p(n)$ may be selected as [23]

$$p(n) = \begin{cases} 1-j & (n = 0,1,.....N_p/2) \\ 1+j & (n = N-N_p/2,.....N-2,N-1) \\ 0 & (otherwise) \end{cases}$$

If the period of *m(k)* is long, then the auto-correlation between *m(k)* tends to be low because the same signal of *m(k)* appears less frequently. Therefore it is better to design *p(n)* so that the period of *m(k)* is long.

From the discussion so far, the new pilot signal design Sine Algorithm steps are as follows when the same pilot signal set is used for all OFDM symbols.

Step 1: Determination of Constants

When the set of the possible values within the fixed constellation is

$$A_M = \{a_0, a_1, a_2, ..., a_{M-1}\}, \text{ let } a = \min_i \mathrm{Re}\{a_i\}, \quad b = \max_i \mathrm{Im}\{a_i\}.$$

Step 2: Design of Pilot Signals

Let $d1$ be the maximum integer smaller than or equal to $2N / N_P$.

$$p(n) = \begin{cases} a - bj & (n = n1 . d1, n1 . d1 + 1, \ \textit{where } 0 \le n \le N/2, \ n1 \textit{is integer}), \\ a + bj & (n = n1 . d1, n1 . d1 + 1, \ \textit{where } N/2 < n \le N\text{-}1, \ n1 \textit{is integer}), \\ 0 & (\textit{otherwise}) \end{cases}$$

To confirm the performance of the newly developed pilot signal, the contribution of the functions $\Lambda_{cp}(\theta)$, $\Lambda_p(\theta)$, and log-likelihood function $\Lambda(\theta)$ is sown in Figure 3.5. Which shows that the magnitude of peaks of $\Lambda_p(\theta)$ at the points other than true time offset are reduced.

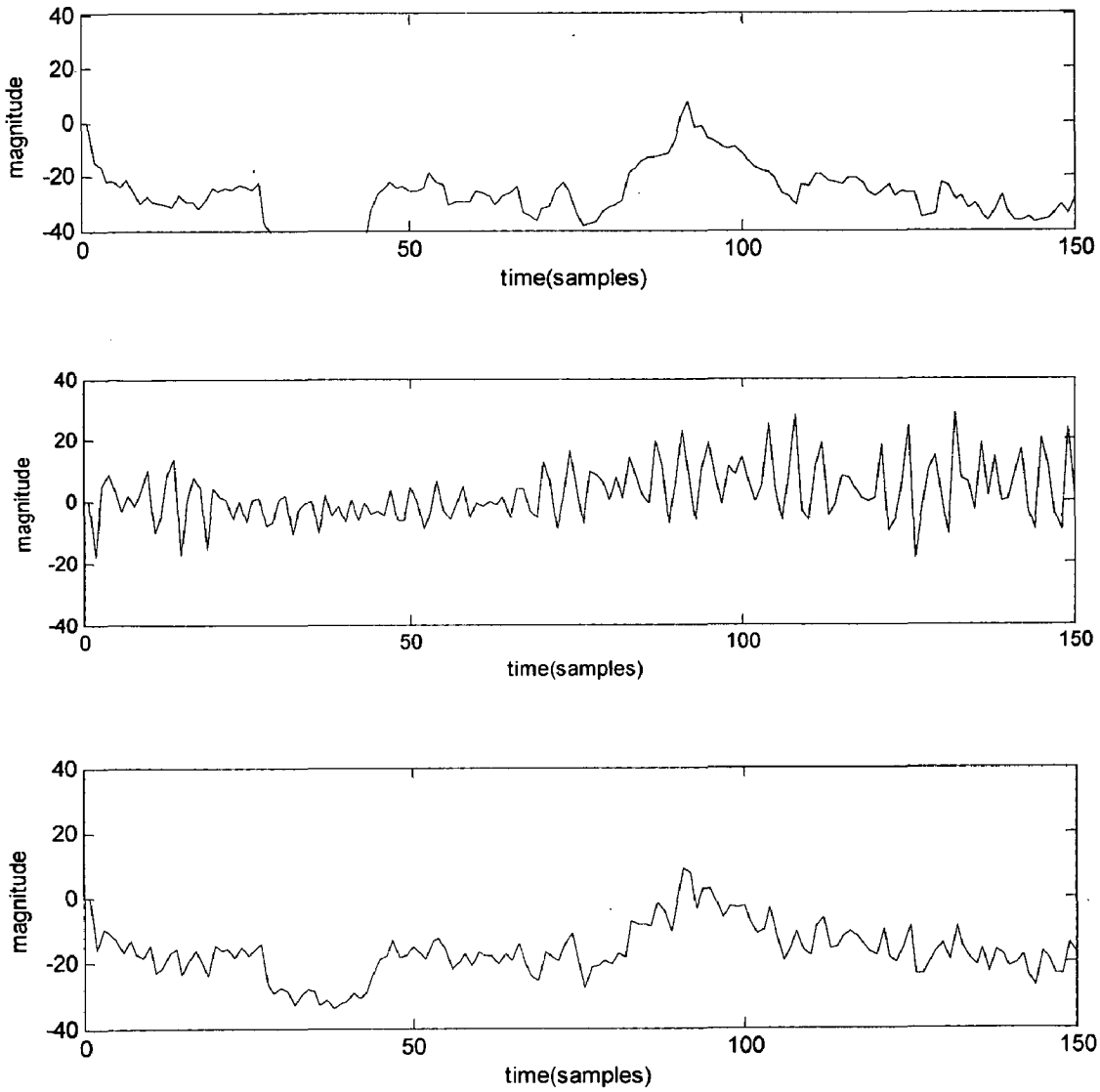

Figure 3.5 The ML estimation statistics in the AWGN channel with pilot signals using Sine Algorithm. Contribution of redundancy of cyclic prefix (top), contribution of pilot signal (middle) resulting log-likelihood function (bottom), one OFDM symbol is $(N+N_g)$=144 samples and *SNR* is 1dB.

Shift Algorithm

Because the length of observation interval of ML estimator for time offset estimation is longer than that of one OFDM symbol, the correlation between (time-domain) pilot signal sets *m(k)* of adjacent OFDM symbols also should be considered. Similarly to the design of the (frequency-domain) pilot signal in one OFDM symbol, the goal is to lower the correlation between the pilot signal sets *m(k)* belonging to adjacent OFDM symbols. Hence, we will follow the fixed process to

select the different pilot signal set for each OFDM symbol. This process can be selected as shifting the pilot signal *p(n)* of the current OFDM symbol cyclically by c (c is the fixed number of samples) and using that cyclically shifted pilot signal $p\left((n-c)\%N\right)$ for the next OFDM symbol. Then let us examine how the IDFT of the shifted pilot signal $p\left((n-c)\%N\right)$ will be by the following equation, where $m_u(k)$ is the (time-domain) pilot signal of u[th] OFDM symbol

$$m_{u+1}(k) = \sum_{n=c}^{N-1+c} p(n-c)\exp\left(j2\pi kn/N\right)$$

$$= \sum_{l=0}^{N-1} p(l)\exp\left(j2\pi kl/N\right)\exp\left(j2\pi kc/N\right)$$

$$= \exp\left(j2\pi kc/N\right)m_u(k). \qquad (3.32)$$

from (3.32), it is that $m_{u+1}(k)$ is different from $m_u(k)$ by the factor of $\exp\left(j2\pi kc/N\right)$, that is phase-different by $2\pi kc/N$ and the effect of which is described in (2.12). Also, for time-dispersive channel, it is desirable that c is larger than the maximum channel delay (when multi-path fading exists) [23]. With this in mind, the steps for the pilot signal design algorithm, when the different pilot signal set is used for each OFDM symbol are,

Step 1: Determination of the Value of c.

Find the maximum channel delay, *d*. Let *c* be the minimum prime number which is greater than *d*.

Step 2: Initialization

Initialize $p_1(n)$ with arbitrary numbers for $0 \le n \le N-1$.

$u \leftarrow 1$.

Step 3: Design of Pilot Signals for the Next OFDM Symbol

$$p_{u+1}(n) = p_u\left((n-c)\%N\right) \quad for\ 0 \le n \le N-1.$$

Step 4: Iteration

$u \leftarrow u+1.$

Repeat *Step 3*.

Sine and Shift Algorithm

From the discussion in the previous algorithms, the two factors need to be considered in designing the pilot signals for efficient ML time offset estimation. First, the periodicity of the (time-domain) pilot signal should be lowered within one OFDM symbol. Second. It is better that the pilot signal set in one OFDM symbol is different from the set in its adjacent OFDM symbols.

Step 1: Determination of Constants

When the set of the possible values within the fixed constellation is $A_M = \{a_0, a_1, a_2, ..., a_{M-1}\}$, let $a = \min_i \mathrm{Re}\{a_i\}$, $b = \max_i \mathrm{Im}\{a_i\}$.

Step 2: Initialization

$u \leftarrow 1$

Let $d1$ be the maximum integer smaller than or equal to $2N / N_P$.

$$p_1(n) = \begin{cases} a-bj & (n = n1 \cdot d1, n1 \cdot d1+1,\ where\ 0 \le n \le N/2,\ n1 is\ integer), \\ a+bj & (n = n1 \cdot d1, n1 \cdot d1+1,\ where\ N/2 < n \le N-1,\ n1 is\ integer), \\ 0 & (otherwise) \end{cases}$$

Step 3: Determination of the Value of c

Find the maximum channel delay, d. Let c be the minimum prime number which is greater than d.

Step 4: Design of Pilot Signals for the Next OFDM Symbol

$$p_{u+1}(n) = p_u\left((n-c)\%N\right) \quad \textit{for } 0 \le n \le N\text{-}1.$$

Step 5: Iteration

$$u \leftarrow u+1.$$

Repeat *Step 4*.

Chapter 4

PERFORMANCE AND SIMULATION RESULTS

In the previous chapter, a brief discussion of various ML based algorithms available in literature for symbol time offset estimation in OFDM was studied. The performance and simulation results are discussed in the following chapter.

Throughout this chapter, the following assumptions are made regarding the OFDM system [3], [9]:

- A cyclic prefix is used.
- The impulse response of the channel is shorter than the cyclic prefix. Otherwise there will be ISI.
- Channel noise is additive, white, and complex Gaussian.
- The fading is slow enough for the channel to be considered constant *during one OFDM symbol interval* unless otherwise mentioned.

4.1 Performance of Cyclic Prefix (CP) Based Estimator

In the analysis we assumed that the channel is non-dispersive and that the transmitted signal *s(k)* is only affected by complex additive white Gaussian noise (AWGN) *n(k)*, i.e., we evaluate our estimator's performance for the AWGN channel.

As discussed in the previous chapter of Section 3.1.2, the ML estimation of time offset is

$$\hat{\theta}_{ML} = \arg\max_{\theta}\{|\gamma(\theta)| - \rho\Phi(\theta)\} \tag{4.1}$$

where

$$\gamma(\theta) = \sum_{k=\theta}^{\theta+N_g-1} r(k)r^*(k+N) \tag{4.2}$$

and

$$\Phi(\theta) = \frac{1}{2}\sum_{k=\theta}^{\theta+N_g-1} |r(k)|^2 + |r(k+N)|^2 \tag{4.3}$$

We can observe from the equation (4.1) that only two quantities affect the performance of the estimator: i.e., the number of samples in the cyclic prefix N_g and the correlation coefficient ρ given by the *SNR*. Basically, the quantity $\gamma(\theta)$ provides the estimate of θ. Its magnitude, which is compensated by an energy term, peaks at time instant $\hat{\theta}_{ML}$.

We use MATLAB simulations to evaluate the performance of the suggested estimator algorithm [11]; we evaluate the performance of the estimators by means of the estimator mean-squared error.

For simulation of cyclic prefix based ML estimator in MATLAB environment, we use the following system parameters:

- No of sub-carriers (FFT size): $N = 256$
- Modulation scheme for source symbols: 16 - QAM
- Observation interval: $(2N+N_g)$ samples
- No of OFDM symbols simulated: nsym = 10,000
- Integer-valued time offset: uniformly distributed over $[0, N+N_g-1]$
- Correlation coefficient: $\rho = \dfrac{SNR}{SNR+1}$

Figure 4.1 shows the flow chart for simulation of cyclic prefix based ML Symbol time offset estimation algorithm.

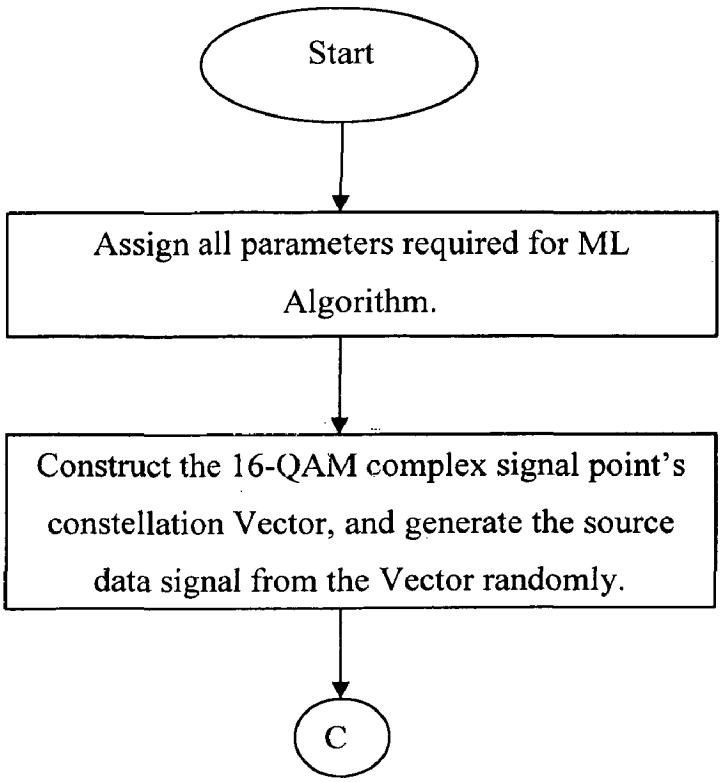

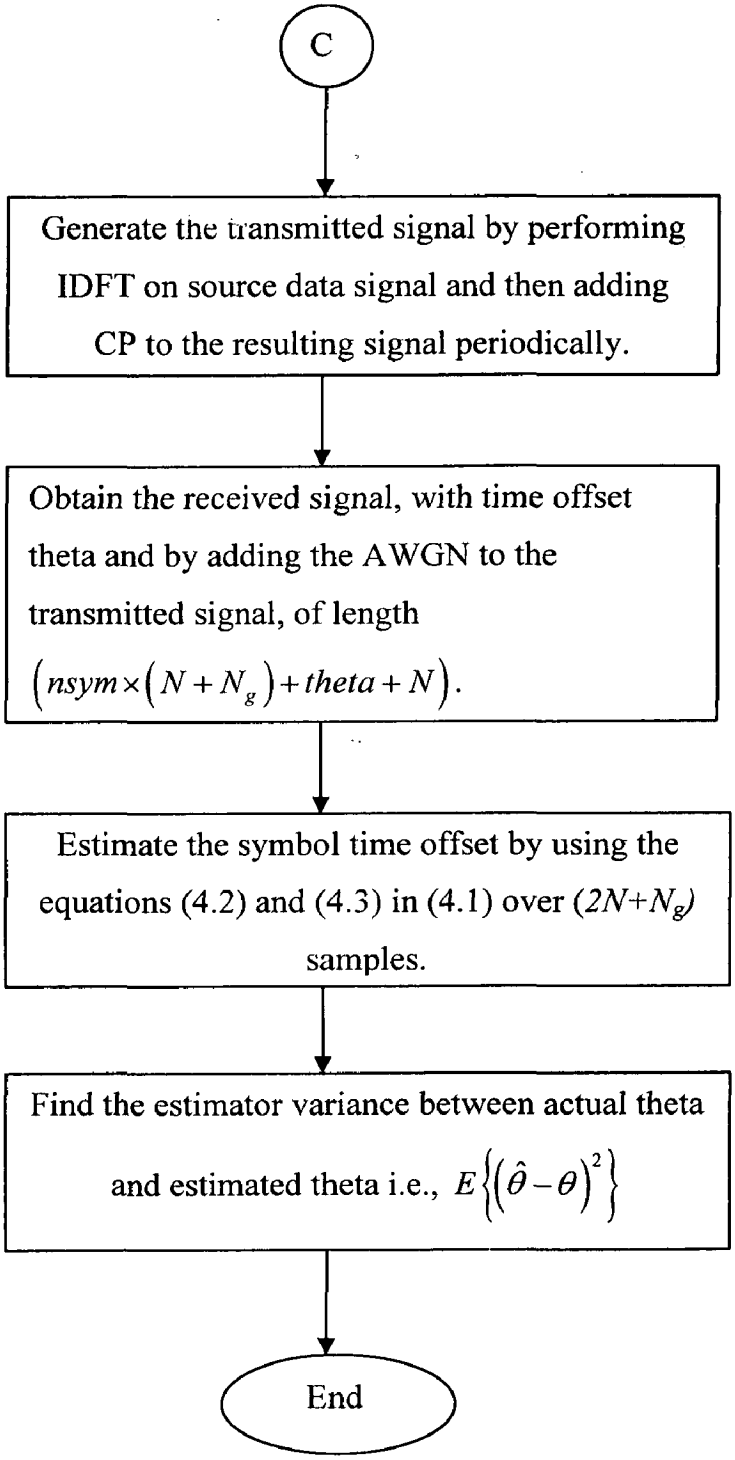

Figure 4.1 Flow chart for simulation of CP based ML algorithm.

Following Figure 4.2 illustraes the index value of the peaks of the estimator in AWGN channel over five OFDM symbols.

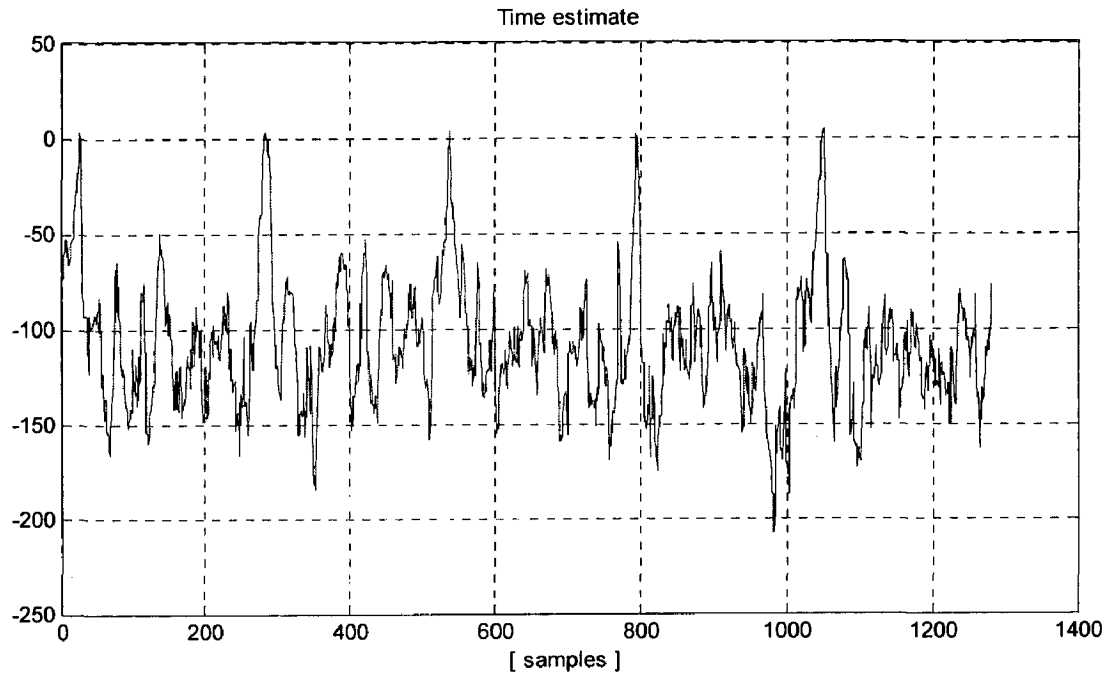

Figure 4.2 signal that generate the ML time estimate ($\hat{\theta}_{ML}$) for ($N = 256$, $N_g = 15$ and $SNR = 16$ dB).

Figure 4.2 shows the essential signal that is generated if a received signal consisting of several OFDM symbols (here, we considered five OFDM symbols) is processed continuously at the receiver by this estimator. The index value of the peaks of this estimator gives the estimation of the time instant $\hat{\theta}$ when the OFDM symbols start.

Following plot shows the performance of the symbol time offset estimator in AWGN channel as a function of length of the cyclic prefix samples, for a fixed values of *SNR*. The parameters are mentioned earlier.

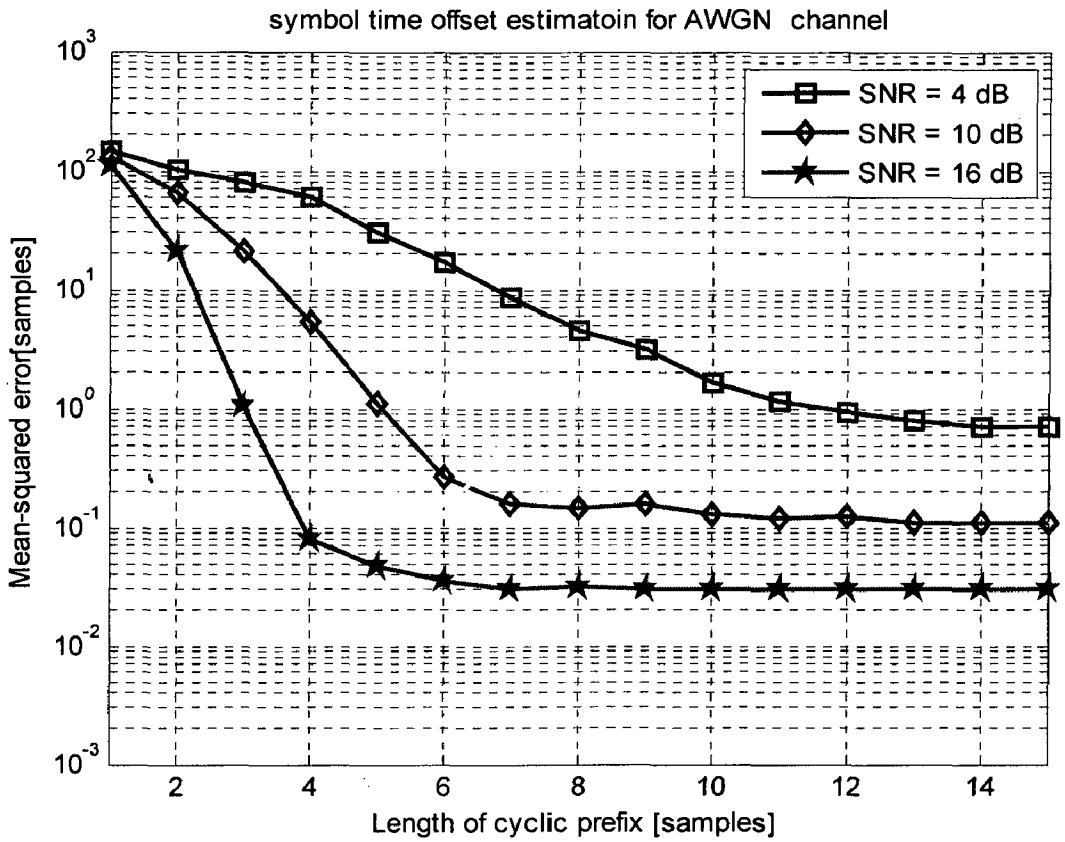

Figure 4.3 Performance of the symbol time estimator for the AWGN channel (4, 10, and 16 dB). The number of sub-carriers is $N = 256$.

This plot shows the performance of the symbol time offset estimator in AWGN channel as a function of *SNR*, for fixed value of CP samples.

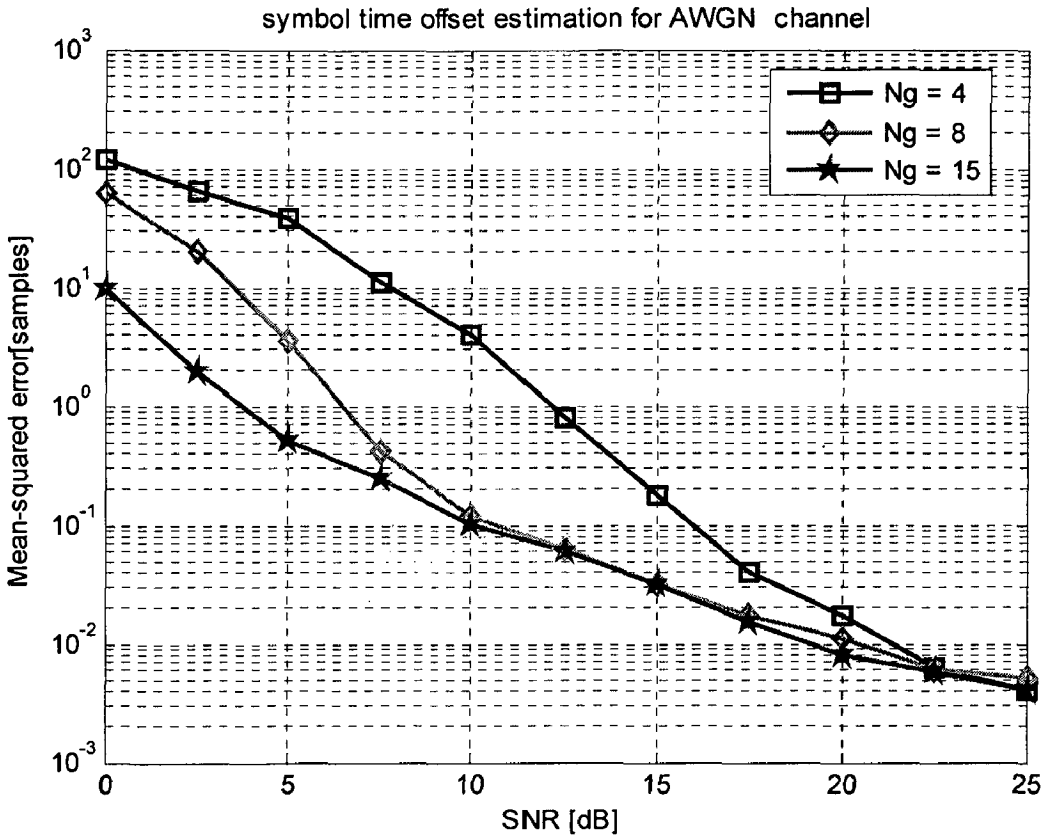

Figure 4.4 Performance of the time estimator for the AWGN channel ($N_g = 4$, $N_g = 8$, and $N_g = 15$). The number of sub-carriers is $N = 256$.

All the steps from starting to the end point of the Figure 4.1 are simulated for 10,000 OFDM symbols at each cyclic prefix length in Figure 4.3 and at each *SNR* in Figure 4.4. Performance results for the AWGN channel are shown in Figure 4.3 and Figure 4.4. First, the estimator mean-squared error as a function of CP length (N_g) is estimated. Figure 4.3 shows the estimator performance for *SNR* values of 4, 10, and 16dB. Notice that the performance of the time estimator is asymptotically independent of N_g, provided that the cyclic prefix is longer than a certain threshold value. This threshold value decreases with the *SNR*. Thus, there is very little advantage in increasing the length of the cyclic prefix beyond the time estimator's threshold [11].

Second, the estimator variance as a function of *SNR* for $N_g = 4$, $N_g = 8$, and $N_g = 15$ are shown in Figure 4.4. Notice that even in this plot, a threshold phenomenon as in Figure 4.3 occurs, but there is advantage in increasing the length of the CP at low *SNR*'s, and the performance improvement as a function of *SNR* is significant [29]. Depending on the application and the presence of a high-performance channel estimator/equalizer, the performance of the time estimate in Figure 4.4 (standard deviation of 1-2 samples) may be good enough to generate a stable clock. In most situations, this performance will suffice at least in an acquisition mode.

4.2 Performance of Hybrid – ML Symbol Time Offset Estimator

In wireless systems, pilots are needed for channel estimation. These pilots can be used by the synchronizer in order to further increase performance. Resulting synchronizers may be hybrid structures using both pilots and the redundancy of the cyclic prefix. How to incorporate pilot symbols in such time and frequency estimators is not straightforward and needs further research.

Another estimation scheme for estimation of symbol time offset is provided in [23], and is discussed in Section 3.1.3 of the previous chapter. This estimation scheme presents novel pilot signal design algorithms for efficient symbol time offset estimation in an OFDM system. As stated in Section 3.1.3 the evenly spaced pilot signals in the frequency- domain have large correlation in the time-domain, and the ML function of the symbol time offset estimator induces an inaccurate value of time offset i.e., the ambiguity is more, in order to avoid this ambiguity to some extent, novel pilot signal design algorithms like Sine Algorithm, Shift Algorithm, and Sine and Shift Algorithm-are developed in terms of positions and values of pilot signals so that the accuracy of the symbol time offset estimator can be improved.

As we already described in equation (3.21), that the received signal *r (k)* is represented by

$$r(k) = s(k-\theta) + m(k-\theta) + n(k) \tag{4.4}$$

The value of θ using ML algorithm can be estimated using two properties of received signal *r (k)*; the statistical properties of the time-domain data signal, *s (k),* and the knowledge of the time-domain pilot signal, *m (k)* over $2N + N_g$ consecutive samples of *r (k).*

The ML estimate θ is acquired by maximizing the log-likelihood function over all possible values of θ.

$$\hat{\theta}_{ML} = \arg\max_{\theta}\{\Lambda(\theta)\} \tag{4.5}$$

$$\Lambda(\theta) = \rho\Lambda_{cp}(\theta) + (1-\rho)\Lambda_{p}(\theta) \tag{4.6}$$

where

$$\Lambda_{cp}(\theta) = \mathrm{Re}\left\{\sum_{k=\theta}^{\theta+N_g-1} r^*(k)r(k+N)\right\} - \frac{\rho}{2}\sum_{k=\theta}^{\theta+N_g-1}\left\{|r(k)|^2 + |r(k+N)|^2\right\} \tag{4.7}$$

exploits the information contained in the redundancy due to the cyclic prefix in the received signal, and

$$\Lambda_p(\theta) = (1+\rho)\,\mathrm{Re}\left\{\sum_k r^*(k)m(k-\theta)\right\} - \rho\,\mathrm{Re}\left\{\sum_{k=\theta}^{\theta+N_g-1}(r(k)+r(k+N))^* m(k-\theta)\right\} \tag{4.8}$$

exploits the information contained in the pilot symbols with ρ given in (3.37).

We use MATLAB simulations to evaluate the performance of the suggested estimator algorithm.

For simulation of hybrid-ML estimator in MATLAB environment, we use the following system parameters:

- No of sub-carriers (FFT size) : $N = 128$
- Length of cyclic prefix (CP): $N_g = 16$
- No of pilot signals: $N_p = 8$
- Alpha $(\alpha) = \dfrac{(N - N_p)}{N}$
- Modulation scheme for source symbols: QPSK
- Observation interval = $(2N+N_g)$ samples
- Integer-valued time offset value: uniformly distributed over [0, $N+N_g$-1]
- No of OFDM symbols simulated: nsym = 10,000

Figure 4.5 shows the flow chart for simulation of hybrid-ML Symbol time offset estimation algorithm

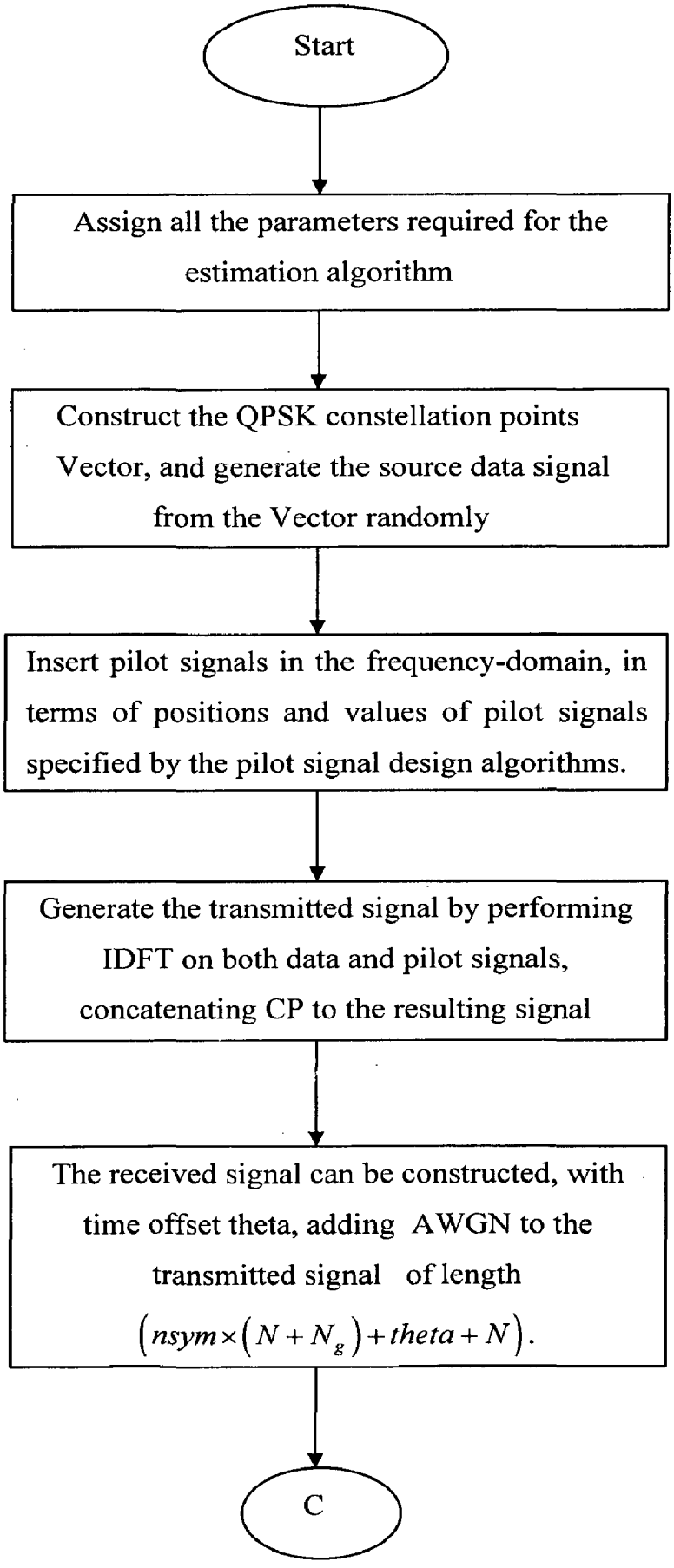

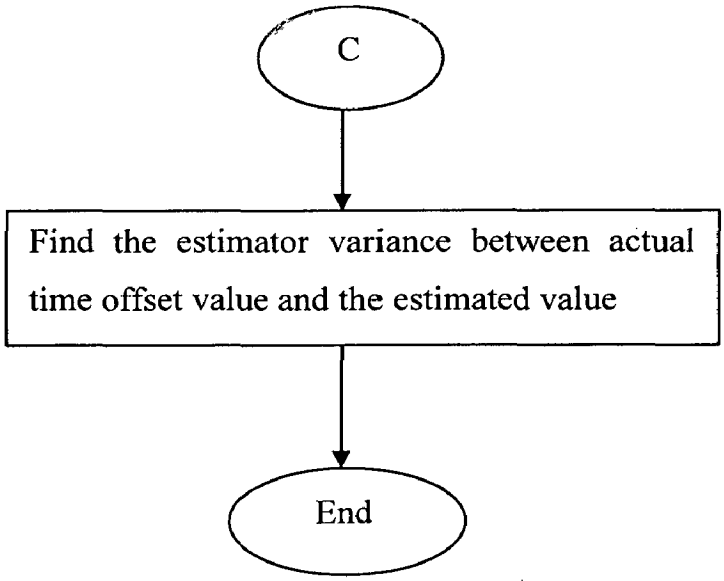

Figure 4.5 Flow chart for simulation of hybrid-ML estimation scheme.

The following figure shows the performance of the symbol time offset estimator for different pilot signals design algorithms (which are discussed in Section 3.1.3) in terms of positions and values for the system parameters mentioned above.

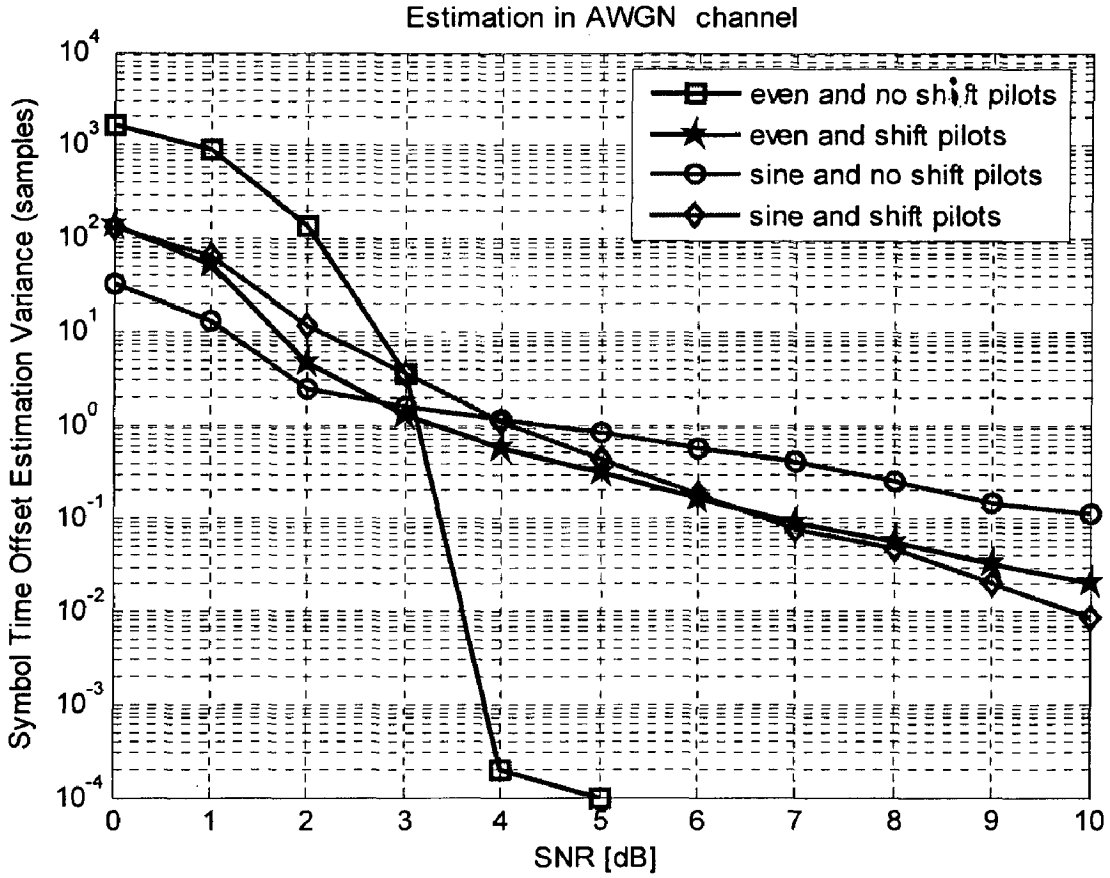

Figure 4.6 The performance of the symbol time offset estimator employing the different pilot signals in the AWGN channel.

Simulation results show the performance of the symbol time offset estimator employing the discussed pilot signal design algorithms in an AWGN channel. The variance of an estimate is used as a performance evaluation parameter. The simulation result in the AWGN channel is shown in Figure 4.6. In the figure "sine and shift pilots", "sine and no shift pilots", "even and shift pilots" employs the pilot signal design algorithms and " even and no shift pilots" employs the pilot signal design algorithm used in the conventional ML symbol time offset estimator [15] , are discussed in Section 3.1.3. As seen in Figure 4.6, for a lower *SNR* than 3dB, the pilot signals employing the novel design algorithm, "Sine" or "Shift" make the symbol time offset estimator variance smaller than the pilot signals employing the conventional design algorithm, "Even and No Shift". While for a higher *SNR* than 3dB, the conventional design algorithm "Even and no Shift" performs better. As indicated in equation (4.6), the pilot signal takes more important roles in the estimation for a low *SNR* than for a high *SNR*. That is the strong points of "Sine" or "Shift" algorithm [23].

As we already discussed in the previous chapter of Section 3.1.3 that $p(n)$ can be chosen such that the (time-domain) pilot signal $m(k)$ becomes similar to low-frequency sine wave. For example, for the QPSK constellation, $p(n)$ may be selected as

$$p(n)=\begin{cases}1-j & (n=0,1,.....N_p/2)\\ 1+j & (n=N-N_p/2,.....N-2,N-1)\\ 0 & (otherwise)\end{cases}$$

and for the 16-QAM constellation, it becomes

$$p(n)=\begin{cases}1-3j & (n=0,1,.....N_p/2)\\ 1+3j & (n=N-N_p/2,.....N-2,N-1)\\ 0 & (otherwise)\end{cases}$$

Since 16-QAM has the smaller real parts of DFT of low-frequency sine wave than QPSK, 16-QAM will perform better, this we can observe from equation (3.31). The simulation plot for these two modulation schemes is shown in Figure 4.7

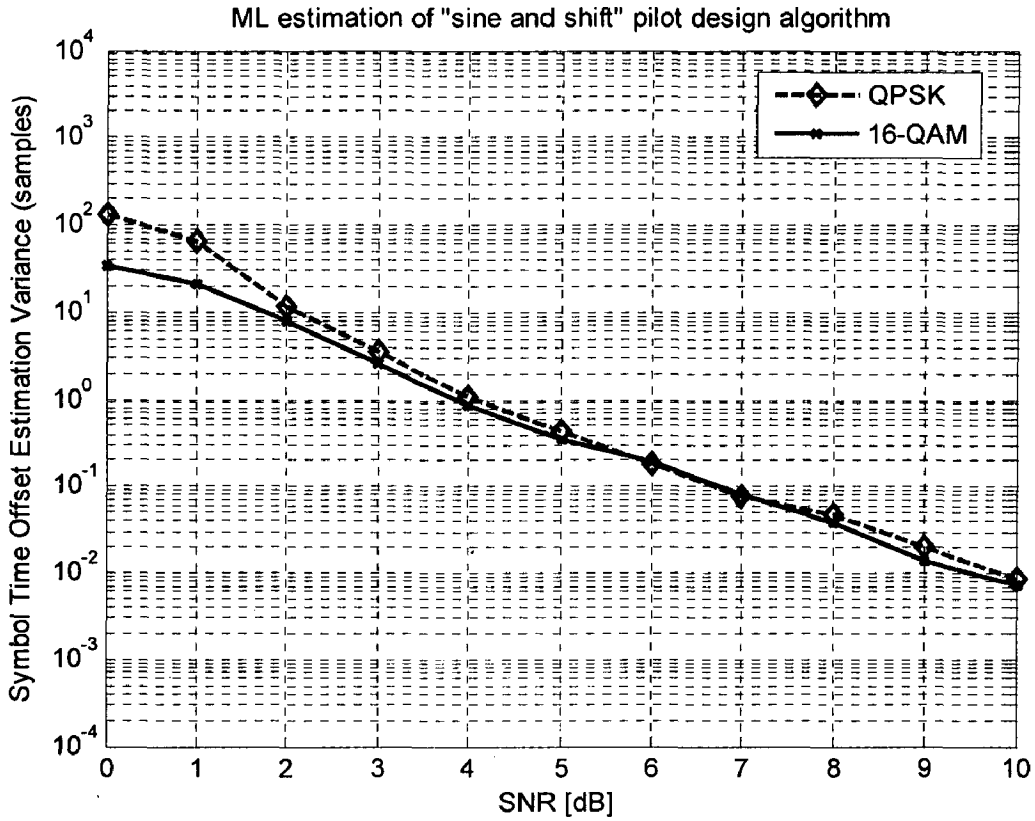

Figure 4.7 The performance of the symbol time offset estimator employing the "Sine and Shift" pilot signal design algorithm for different modulation schemes in AWGN channel.

From the Figure 4.7 we can observe that the 16-QAM modulation scheme will give better results than the QPSK modulation scheme, and the above plot shows large variance difference about 44.42 samples at 1 dB *SNR* and small difference about 0.0101 at 8 dB *SNR* value, as we expected for pilot signal design algorithms.

4.2.1 Rayleigh Fading Channel

Rayleigh fading is a statistical model for the effect of a propagation environment on a radio signal such as that used by wireless devices. It assumes that the power of a signal that has passed through such a transmission medium (also called a communication channel) will vary randomly or fade according to a Rayleigh distribution. Rayleigh fading is most applicable when there is no line of sight between the transmitter and receiver [30].

In a multipath propagation environment, the received signal is sometimes weakened or intensified. The signal level of the received wave changes from moment to moment. Multipath fading raises the error rate of the received data. This section discusses the concept of multipath fading and explains a programming method for simulations of multipath fading.

The path between base station and mobile stations of terrestrial mobile communications is characterized by various obstacles and reflections. The delayed wave with incident angle θ_n is given by the following equation (4.9) and, when a continuous wave of single frequency f_c is transmitted from the base station.

$$r_n(t) = \mathrm{Re}\left[e_n(t)\exp j(2\pi f_c t)\right] \tag{4.9}$$

where Re[ ] indicates the real part of a complex number that gives the complex envelope of the incoming wave from the direction of the number n and $e_n(t)$ is given in (4.10) by using propagation path length from the base station of the incoming waves: L_n, the speed of the mobile station, v, and the wavelength, λ

$$\begin{aligned} e_n(t) &= R_n(t)\exp j\left(-\frac{2\pi(L_n - vt\cos\theta_n)}{\lambda} + \phi_n\right) \\ &= x_n(t) + jy_n(t) \end{aligned} \tag{4.10}$$

where R_n and ϕ_n are the envelope and phase of the n^{th} incoming wave. $x_n(t)$ and $y_n(t)$ are the in-phase and quadrature-phase factors of $e_n(t)$, respectively. The incoming n^{th} wave shifts the carrier frequency as $\frac{v\cos\theta_n}{\lambda}$ (Hz) by the Doppler effect. This is called the Doppler shift [31], which described as f_d, has a maximum

value of $\frac{v}{\lambda}$, when the incoming wave comes from the running direction of the mobile station in $\cos\theta_n = 1$. Then this maximum is the largest Doppler shift. The delayed wave that comes from the rear of the mobile station also has a frequency shift of $-f_d$. Since received wave $r(t)$ received in the mobile station is the synthesis of the above-mentioned incoming waves, when the incoming wave number is made to be M it is shown by (4.9), .

$$
\begin{aligned}
r(t) &= \sum_{n=1}^{M} r_n(t) \\
&= \mathrm{Re}\left[\left(\sum_{n=1}^{M} e_n(t)\right)\exp j(2\pi f_c t)\right] \\
&= \mathrm{Re}\left[\left(x(t)+jy(t)\right)\left(\cos 2\pi f_c t + j\sin 2\pi f_c t\right)\right] \\
&= x(t)\cos 2\pi f_c t - y(t)\sin 2\pi f_c t
\end{aligned} \tag{4.11}
$$

where

$$
x(t) = \sum_{n=1}^{M} x_n(t)
$$

$$
y(t) = \sum_{n=1}^{M} y_n(t) \tag{4.12}
$$

and $x(t)$ and $y(t)$ are normalized random processes, having an average value of 0 and dispersion of σ, when M is large enough. The combination probability density $p(x,y)$ is then given by (4.13), where $x = x(t)$, $y = y(t)$

$$
p(x,y) = \frac{1}{2\pi\sigma^2}\exp\left(\frac{x^2+y^2}{2\sigma^2}\right) \tag{4.13}
$$

In addition, it can be expressed as $r(t)$ using the amplitude and phase of the received wave.

$$
r(t) = R(t)\cos\left(\cos 2\pi f_c t + \theta(t)\right) \tag{4.14}
$$

$R(t)$ and $\theta(t)$ are given by

$$
\begin{aligned}
R(t) &= R = \sqrt{x^2+y^2} \\
\theta(t) &= \theta = \tan^{-}[y/x]
\end{aligned} \tag{4.15}
$$

By using a transformation of variables, $p(x,y)$ can be converted into $p(R,\theta)$

$$p(R,\theta)=\frac{R}{2\pi\sigma^2}\exp\left(-\frac{R^2}{2\sigma^2}\right) \tag{4.16}$$

By integrating $p(R,\theta)$ over θ from 0 to 2π, the probability density function $p(R)$ is obtained (4.17).

$$p(R)=\frac{R}{\sigma^2}\exp\left(-\frac{R^2}{2\sigma^2}\right) \tag{4.17}$$

By integrating $p(R,\theta)$ over R from 0 to ∞, the probability density function $p(\theta)$ is obtained (4.18).

$$P(\theta)=\frac{1}{2\pi} \tag{4.18}$$

From these equations (4.17) and (4.18), the envelope fluctuation follows a Rayleigh distribution, and the phase fluctuation follows a uniform distribution on the fading in the propagation path.

An expression for simulations of this Rayleigh fading is found in [31] i.e., the complex fading fluctuation in an equivalent low pass system is

$$\begin{aligned} r(t) &= x(t)+j.y(t) \\ &= \left[\sqrt{\frac{2}{M_1+1}}\sum_{n=1}^{M_1}\sin\left(\frac{\pi n}{M_1}\right)\cos\left\{2\pi f_d\cos\left(\frac{2\pi n}{M_1}\right)t\right\}+\frac{1}{\sqrt{M_1+1}}\cos(2\pi f_d t)\right] \\ &\quad +j\sqrt{\frac{2}{M_1}}\sum_{n=1}^{M_1}\sin\left(\frac{\pi n}{M_1}\right)\cos\left\{2\pi f_d\cos\left(\frac{2\pi n}{M_1}\right)t\right\} \end{aligned} \tag{4.19}$$

where M_1 is given by

$$M_1=\frac{1}{2}\left(\frac{M}{2}-1\right)$$

In this case, the following relations are satisfied

$$E\left[x_I^2(t)\right]=E\left[x_Q^2(t)\right]=\frac{1}{2}$$

$$E\left[x_I(t)y_Q(t)\right]=0 \tag{4.20}$$

and it is shown that the result of (4.19) takes the form of program in Appendix C with sub function name *fade.m,* which generates Rayleigh fading.

Next, let us discuss how a multipath propagation environment can be simulated. In the multipath propagation environment, the mobile station receives not only the direct wave but also delayed waves caused by reflection, diffraction, and scattering that reach the time later than the direct wave. The model of the relationship between this direct wave and the delayed wave is shown in Figure 4.8 [30]

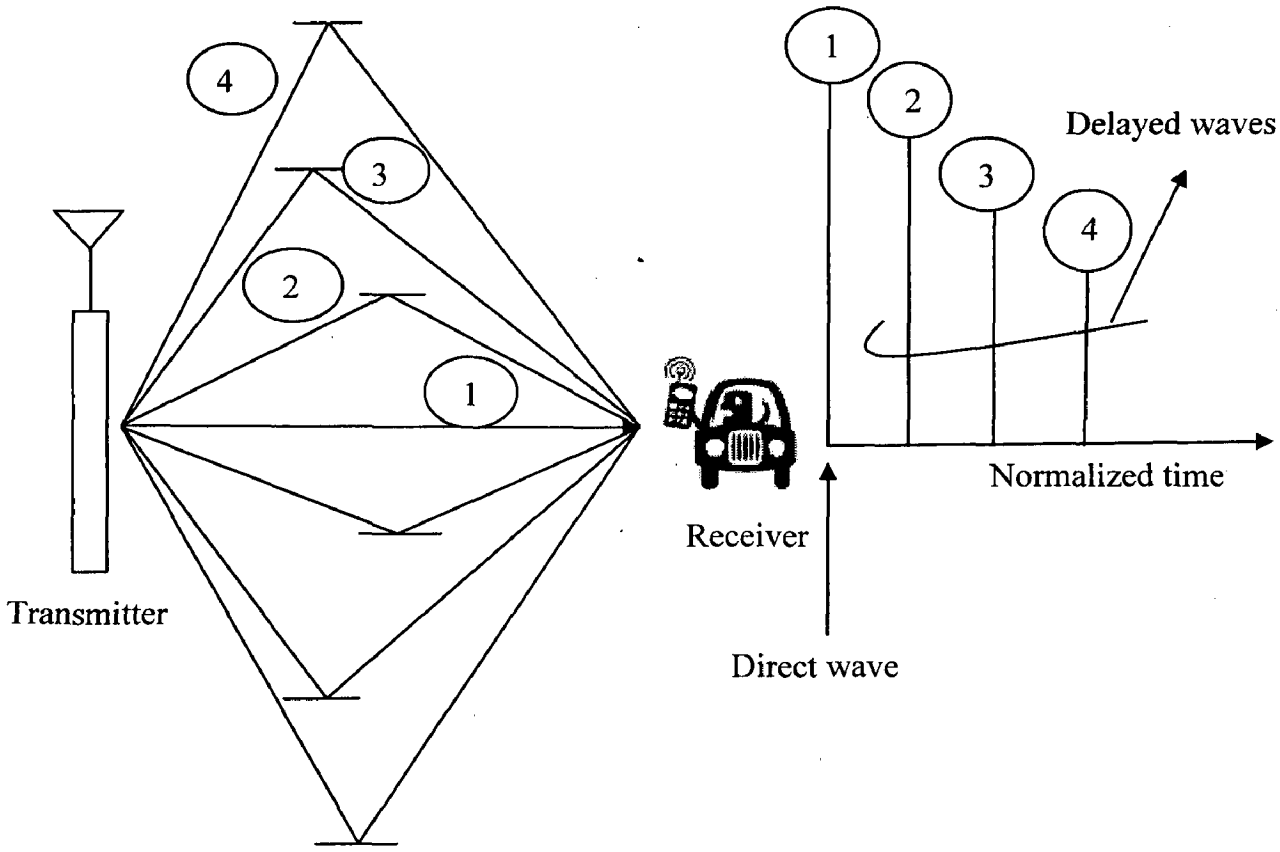

Figure 4.8 Configuration of multipath fading channel

It is clear that the amplitude has a Rayleigh distribution and that the phase has a uniform distribution when the received signal is observed at the arrival time. It is also clear that there are fixed ratios of the average electric powers of the direct and delayed waves. Therefore, in simulating multipath fading environment, only the relative signal level and relative delay time of the delayed waves need to be given in comparison with the direct wave [30], when this multipath propagation environment

is simulated; its flowchart is shown in Figure 4.9. The Matlab function for simulations of multipath fading is given in Appendix C.

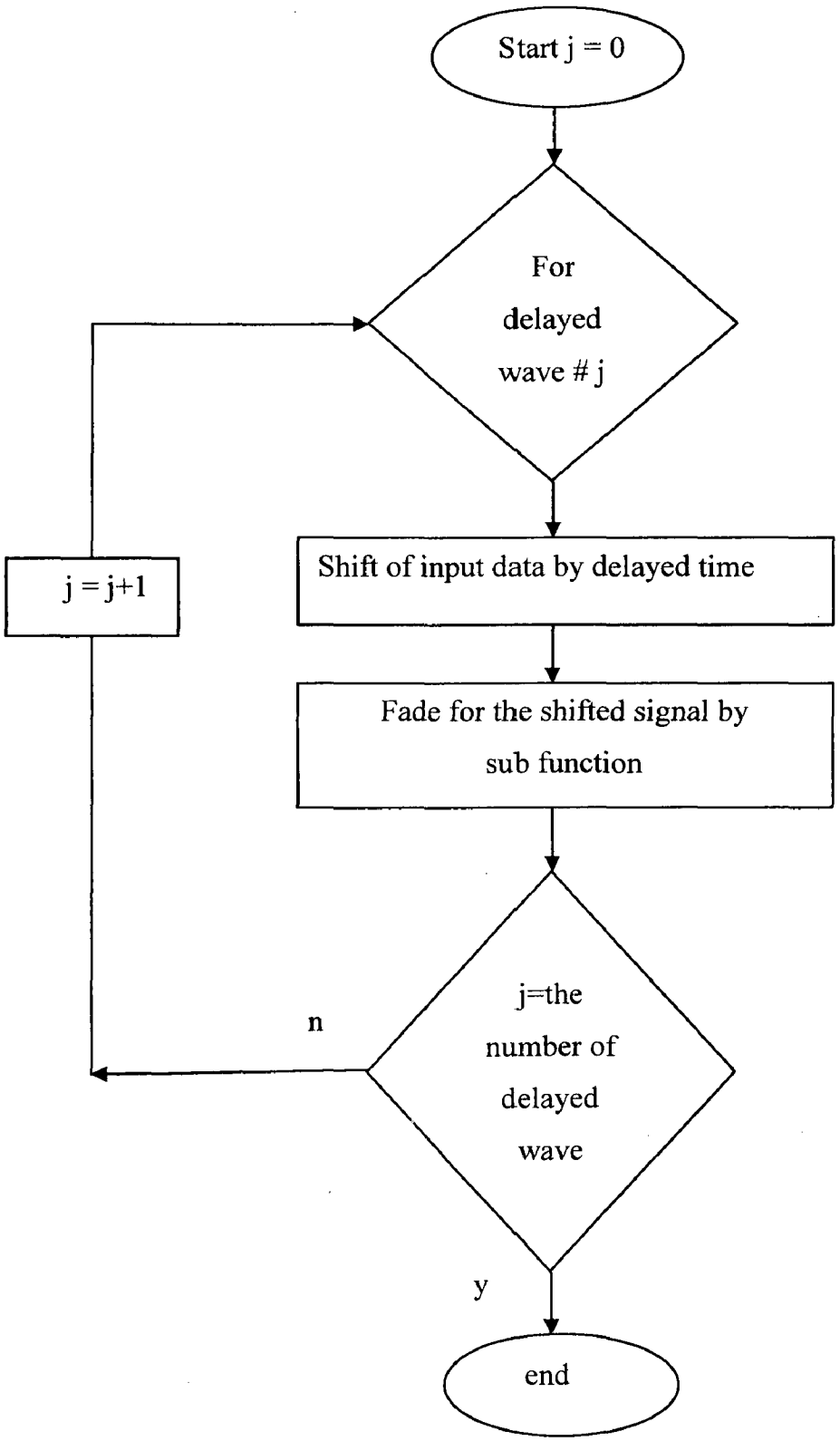

Figure 4.9 Flow chart to obtain multipath fading channel

Based on the flowchart, the Matlab functions are written for the multipath fading. The function (*C*.1) in Appendix C is the fading sub function to shift the input data by the specified delayed time. Second function (*C*.2) performs the entire flowchart above and calls two sub functions-delay.m and fade.m to achieve the multipath fading channel. The inputs are the time resolution, relative signal levels and relative delay times of the direct and delayed waves and the simulation time for one simulation loop.

Consider, as an example, the case of a simulation time at one simulation loop and a minimum time resolution of simulation use $50\mu s$ and $0.5\mu s$, respectively. It is assumed that three delayed waves have mean powers of 10 dB, 20 dB, and 25 dB smaller than that of the direct wave, respectively, and that the relative arrival times were retarded with respect to the direct wave by 1, 1.5, and $2.0\,\mu s$, respectively. In this case, the input variable for the multipath fading simulator [30] is

```
tstp = 0.5.*10.^(-6);
itau = [0 floor(1.*10.^(-6)/tstp) floor(1.5.*10.^(-6)/tstp) floor(2.0.*10.^(-6)/tstp)]
     = [0, 2, 3, 4];
dlvl = [0,10, 20,25];
```

The parameter is set using such expressions for the simulator. Next, we describe the operation of the multipath fading simulator. The Frequency selecting fading function (*C*.3) begins by delaying the input signal by using the above input parameters. Next, Rayleigh fading is added to the delayed signals, and only the number of delayed waves set in the parameter repeats this process. All are added afterwards. As a result, the output signal taken from the multipath Rayleigh fading is obtained.

A fading counter method is used here for generating an independently fading delay time. The fading counter gives the start time of fading generation to a fading generator such as fade.m. Different start times of fading generation must be set to all direct and delayed waves to simulate an independently distributed Rayleigh fading environment.

Now, we present the performance of the symbol time offset estimator employing the pilot signal design algorithms discussed in (Section 3.1.3) for the above discussed channel, by considering the following system parameters. Consider

the channel consisting of 8 taps is independently fading [23], as discussed above and it is quasi-static so that it is constant over one OFDM symbol.

The system parameters are:

- Number of sub-carriers (FFT size): $N = 128$
- Length of cyclic prefix (CP): $N_g = 16$
- No of pilot signals: $N_p = 25$
- Alpha $(\alpha) = \frac{(N - N_p)}{N}$
- Modulation scheme for source symbols: QPSK
- Observation interval = $(2N+N_g)$ samples
- Integer-valued time offset value: uniformly distributed over [0, $N+N_g$-1]
- No of OFDM symbols simulated: nsym = 10,000
- Time resolution tstp = $0.1\mu s$
- Doppler frequency $f_d = 50Hz$
- Number of simulation loop (nloop) = 1000
- Number of taps $t_p = 8$
- Number of fading counters = 8
- Delay times: itau = [0, 1, 2, 3, 4, 5, 6, 7]
- Signal attenuation levels in dB : dlvl = [0, 7, 14, 21, 28, 35, 42, 49]

Figure 4.10 and Figure 4.11 shows that the pilots employing any one of "Sine" algorithm and "Shift" algorithm at Doppler frequencies (f_d = 50 Hz) and (f_d = 60 Hz) respectively, perform better than the pilots employing the conventional equally spaced pilots, referred to as "Even and no Shift" algorithm, for a lower *SNR* than 5dB.

Comparing Figure 4.6 with Figure 4.10, we find that the presented pilot signal design algorithm performs better in time-dispersive channel with a great performance gain. Especially, the pilot signal which employs "Shift algorithm performs good compared with the pilot signal which does not employ it over the wide *SNR* range.

Figure 4.12 shows performance of the pilots employing "Sine and no Shift" algorithm for two different Doppler frequencies and it is observed that at 5dB *SNR*

the estimator shows 0.475 error for 50 Hz Doppler frequency and 0.9035 error for 60 Hz Doppler frequency.

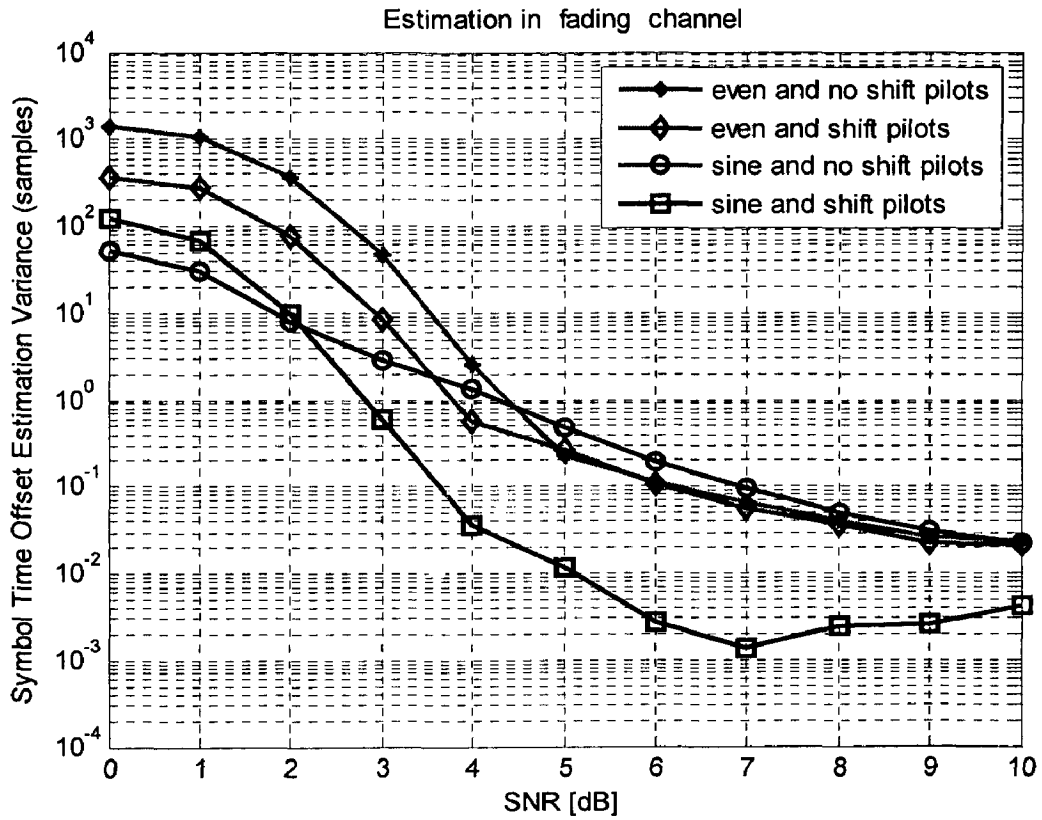

Figure 4.10 The performance of the symbol time offset estimator employing the several different pilot signals in a dispersive channel, at Doppler frequency ($f_d = 50Hz$).

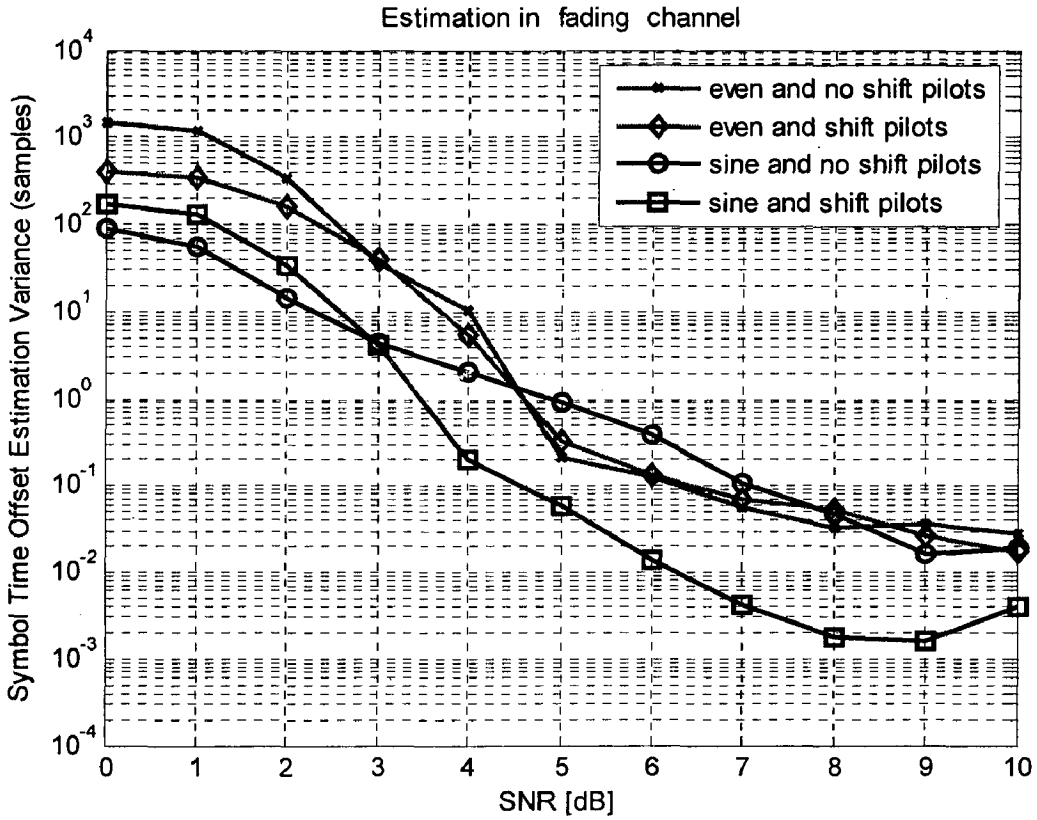

Figure 4.11 The performance of the symbol time offset estimator employing the several different pilot signals in a dispersive channel, at Doppler frequency (f_d= 60 *Hz*).

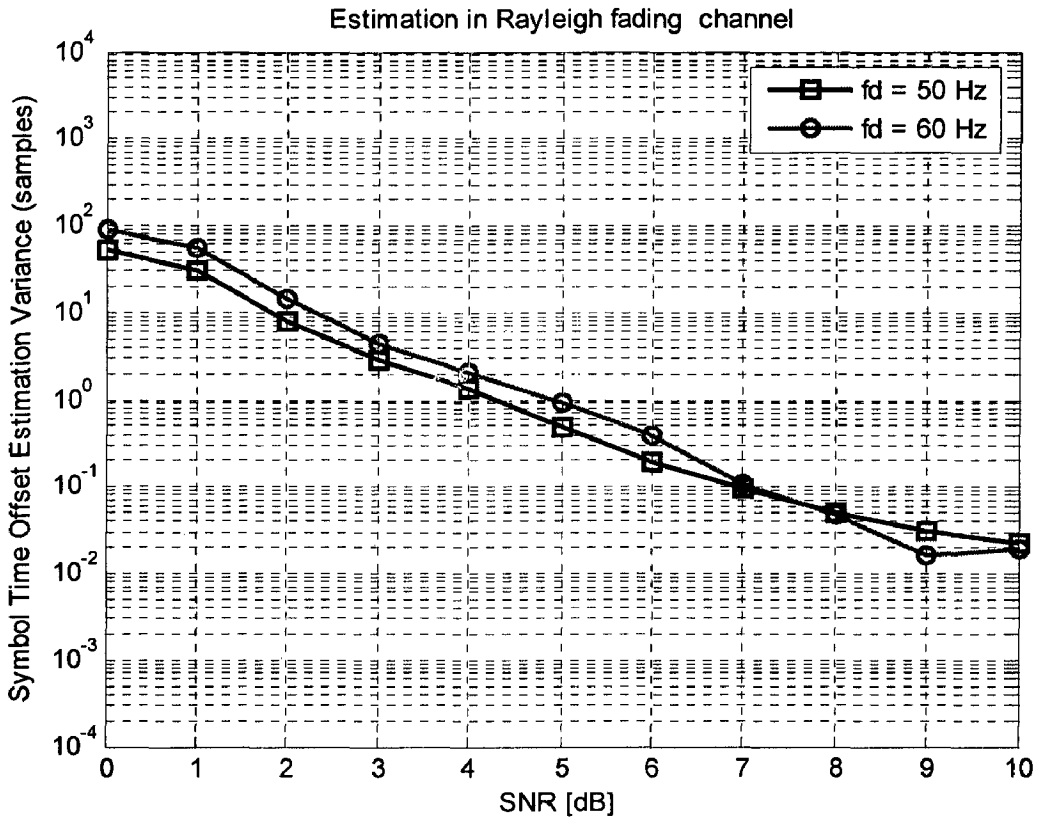

Figure 4.12 The performance of the symbol time offset estimator employing the "Sine and no Shift" pilot signals in a dispersive channel, at two Doppler frequencies ($f_d = 50Hz,\ 60Hz$).

Chapter 5
CONCLUSIONS

The performance of a wireless receiver is measured by its ability to successfully receive transmitted information. In the context of wireless communications, the baseband signal processing algorithms generally assume perfect synchronization. In practical systems, however, synchronization at the receiver is a critical aspect that impacts the performance of the entire system. Before actual processing and decoding of the received data can occur, synchronization needs to be considered. The receiver signal processing blocks downstream depends on this and consequently is susceptible to errors in synchronization.

In this thesis, we have addressed the problem of symbol timing estimation for OFDM systems. This dissertation work was aimed at studying the application and performance of various timing offset estimation schemes in OFDM systems, which has use the blind algorithms with extension of cyclic prefix samples and the hybrid structures using both pilots and the redundancy of the cyclic prefix.

Cyclic Prefix Based ML Timing Estimation for OFDM Systems

We have presented the ML estimation of time offset. It uses the redundant information contained within the cyclic prefix. It is derived under the assumption that the channel distortion only consists of additive noise, the simulations shows that the estimator mean-squared error as a function of cyclic prefix is asymptotically independent of CP length, provided that the cyclic prefix is longer than a certain threshold. This threshold value decreases with the increasing *SNR* (i.e., for 4dB, 10dB, and 16dB *SNR's* N_g = 13, N_g = 8 and N_g = 6 samples, respectively are the threshold values in Figure 4.3). Also the estimator error as a function of *SNR* for N_g = 4, 8 and 15 samples, shows a continuous performance improvement for wide range of *SNR's,* even there is a threshold phenomenon of CP lengths. (i.e., from 10dB *SNR* onwards, the estimator gives the similar performance almost, as shown in Figure 4.4, for N_g= 8, and 15 samples).

Hybrid-ML Estimation for OFDM Systems

In wireless systems, pilots are needed for channel estimation. These pilots can be used by the synchronizer in order to further increase performance. Resulting synchronizer is the hybrid structure using both pilots and the redundancy of the cyclic prefix. How to incorporate pilot symbols in such time estimators is an important challenging design parameter.

Evenly spaced pilot signals in the frequency-domain which were used in the conventional symbol time offset estimator can induce ML function used in the estimation process to have an inaccurate value of time offset. They have large correlations between the time-domain pilot signals in addition to correlations due to the cyclic prefix.

The presented pilot signal design algorithms were devised to solve these problems. Sine algorithm is developed for the case that the same pilot signal set is used for all OFDM symbol and Shift algorithm is for the case that the different pilot signal set is used for each OFDM symbol. From the simulation results, for a lower *SNR* than 3 dB the pilot signals employing the pilot design algorithms make the symbol time offset estimator variance smaller than the pilot signals employing the conventional design algorithms. While for higher *SNR* than 3 dB the conventional design algorithms performs better.

In a time dispersive channel, the pilot signal design algorithm performs with a better gain. Especially, shift algorithm performs good compared with the pilot signal which does not employ it.

Scope of Future Work

In this desertion work, symbol timing estimation is done using both CP and pilots. Most schemes at present deal with the synchronization and the channel estimation separately. In fact, the channel estimation may be severely affected by the residual synchronization errors, and in view of system design optimization point of view, these two operations should be considered jointly.

REFERENCES

[1] Shinsuke Hara, Ramjee Prasad, "Multicarrier Techniques for 4G Mobile Communications," Artech House, 2003.

[2] Theodore S. Rappaport, "Wireless Communications," 2nd edition, Eastern Economy Edition, 2006.

[3] Mohinder Janikiraman, "Space-time codes and MIMO systems," Artech House, pp.155-207, 2004.

[4] J. G. Proakis, "Digital Communications," 4th edition, McGraw-Hill, 2003.

[5] W. Y. Zou, and Y. Wu, "COFDM: An overview," IEEE Transactions on Broad-casting, vol. 41, pp.1-8, Mar 1995.

[6] J. A. C. Bingham, "Multicarrier modulation for data transmission: An idea whose time has come," IEEE Communication Magazine, vol. 28, pp.5-14, May 1990.

[7] N. Chen, M. Tanaka and R. Heaton, "OFDM Timing Synchronization Under Multi-path Channels," in IEEE VTC, vol. 1, pp.378-382, April 2003.

[8] Hao Zhou, A. V. Malipatil, Yih-Fang Huang, " Synchronization Issues in OFDM Systems," IEEE Asia Pasific Conference on Circuits and Systems, APCCAS2006, pp.988-991, Dec 2006.

[9] M. Speth, S. Fechtel, G. Fock, and H. Meyr, "Optimum Receiver Design for Wireless Broad-Band Systems Using OFDM-Part I," IEEE Transactions on Communication, vol. 47, Issue: 11, pp.1668-1677, Nov 1999.

[10] M. Speth, S. Fechtel, G. Fock, and H. Meyr, "Optimum Receiver Design for OFDM-based Broadband Transmission-Part II: A case Study," in IEEE Transactions on Communication, vol. 49, Issue: 4, pp.571-578, April 2001.

[11] J. J. Van de Beek, M. Sandell, and P. O. B¨orjesson, "ML estimation of time and frequency offset in OFDM systems," IEEE Transactions on Signal Processing, vol. 45, pp.1800-1805, July 1997.

[12] J. Lee, H. Lou, and D. Toumpakaris, "Maximum likelihood estimation of time and frequency offset for OFDM," Electronics Letters, vol. 40, pp.1428-1429, Oct 2004.

[13] T. M. Schmidl and D. C. Cox, "Robust frequency and timing synchronization for OFDM," IEEE Transaction on Communications, vol. 45, Issue: 12, pp.1613-1621, Dec 1997.

[14] H. Minn, V. K. Bhargava, M. Zeng, "On timing offset estimation for OFDM systems," IEEE Communications Letters, vol. 4, Issue: 7, pp.242-244, July 2000.

[15] D. Landström, S. K. Wilson, J. J. Van de Beek, P. Ödling, and P. O. Börjesson, "Symbol time offset estimation in coherent OFDM systems," IEEE International Conference on Communications, pp.500–505, June 1999.

[16] C. R. N. Athaudage, "BER sensitivity of OFDM systems to time synchronization error," 8th IEEE International Conference on Communication Systems, pp.42-46, Nov 2002.

[17] M. Speth, F. Classen, and H. Meyr, "Frame synchronization of OFDM systems in frequency selective fading channels," in Proceedings of the IEEE Vehicular Technology Conference VTC, pp.1807-1811, 1997.

[18] Lee, J. Toumpakaris, D. Lou, H. -L., "Optimum Symbol Timing Estimation with Various Performance Measures for OFDM Systems," IEEE International Conference on Communications, vol. 3, pp.1969-1973, 2005.

[19] A. J. Coulson, "Maximum Likelihood synchronization for OFDM using a pilot symbol: Algorithms," IEEE Journal on Selected Areas in Communication, vol. 19, Issue: 12, pp. 2486-2494, Dec 2001.

[20] T. Pollet and M. Moeneclaey, "Synchronizability of OFDM signals," in Proceeidngs Globecom'95, Singapore, vol. 3, pp.2054-2058, Nov 1995.

[21] D. Lee and K. Cheun, "Coarse Symbol Synchronization Algorithms for OFDM Systems in Multipath Channels," IEEE Communication Letters, vol. 6, Issue: 10, pp.446-448, Oct 2002.

[22] H. Minn, V. K. Bhargava, " A simple and efficient timing offset estimation for OFDM systems," IEEE 51st Vechiular Technology Conference Proceedings, vol. 1, pp.51-55, 2000.

[23] S. B. Hong, H. -M. Kim, "Pilot signal design algorithm for efficient symbol time offset estimation in an OFDM system," Signal Processing, pp. 489-499, July 2007.

[24] B. Yang, K. B. Letaief, R. S. Cheng, and Z. Cao, "Timing Recovery for OFDM Transmission," in IEEE journal on Selected Areas in Communications, vol. 18, Issue: 11, pp.2278-2291, Nov 2000.

[25] E. G. Larsson, Guoqing Liu, Jain Li, and G. B. Giannakis, "Joint symbol timing and channel estimation for OFDM based WLANs," IEEE Communications Letters, vol. 5, Issue: 8, pp. 325-327, Aug 2001.

[26] A. J. Coulson, "Maximum likelihood synchronization for OFDM using a pilot symbol: Analysis," IEEE Journal on Selected Areas in Communication, vol. 19, pp.2495-2503, Dec 2001.

[27] J. -J. Van de Beek, M. Sandell, M. Isaksson, and P. Borjesson, "Low-complex frame synchronization in OFDM systems," in Proceedings ICUPC, pp.982-986, Nov 1995.

[28] Tiejun Lv, Jie Chen, "ML estimation of timing and frequency offset using multiple OFDM symbols in OFDM systems," IEEE GLOBECOM '03, Global Telecommunications Conference, vol. 4, pp.2280-2284, Dec 2003.

[29] G. C. Carter, "Coherence and time delay estimation," Proceedings IEEE, vol. 75, pp.236-255, Feb 1987.

[30] Hiroshi Harada, Ramjee Prasad, "Simulation and Software Radio for Mobile Communications," Artech House, pp.29-69, New York, USA 2002.

[31] Jakes, W. C., "Microwave Mobile Communications," New York: IEEE Press, 1994.

Appendix A

Derivation of Symbol Time and Frequency Offset Estimation for Cyclic Prefix Based Scheme

Details of the derivation of the algorithm described in Section 3.1.2 is provided here. Since the last N_g samples of the transmitted signal are same as the first N_g samples, the correlation of received signal $r(k)$ can be given as

$$E\{r(k)r^*(k+m)\} = \begin{cases} \sigma_s^2 + \sigma_n^2 & m = 0 \\ \sigma_s^2 e^{-j2\pi\varepsilon} & m = N \\ 0 & otherwise \end{cases} \quad (A.1)$$

The log-likelihood functions for θ and ε, $\Lambda(\theta,\varepsilon)$ is the logarithm of the probability density function $f(\mathbf{r}/\theta,\varepsilon)$ of the $2N+N_g$ observed samples in vector **r** given the arrival time θ and the carrier frequency offset ε. In the following, we will drop all additive and positive multiplicative constants that show up in the expression of the log-likelihood function since, they do not affect the maximizing argument. Using the correlation properties of the observation **r**, the log-likelihood function can be written as

$$\begin{aligned} \Lambda(\theta,\varepsilon) &= \log f(\mathbf{r}/\theta,\varepsilon) \\ &= \log\left(\prod_{k\in I} f(r(k),r(k+N)) \prod_{k\notin I\cup I'} f(r(k))\right) \\ &= \log\left(\prod_{k\in I} \frac{f(r(k),r(k+N))}{f(r(k))f(r(k+N))} \prod_k f(r(k))\right) \end{aligned} \quad (A.2)$$

where $f(.)$ denotes the probability density function of the variables in its argument. Notice that it is used for both one and two-dimensional (1-D and 2-D) distributions. The product $\prod_k f(r(k))$ in (A.2) is independent of θ (since product is over all k) and ε (since the density $f(r(k))$ is rotationally invariant).since the ML estimation of θ and ε is the argument maximizing $\Lambda(\theta, \varepsilon)$, we may omit this factor. Under the assumption that **r** is a jointly Gaussian vector, and (A.2) can be shown as [11]

$$\Lambda(\theta,\varepsilon)=\sum_{k=\theta}^{\theta+N_g-1}\log\left(\frac{f(r(k),r(k+N))}{f(r(k))f(r(k+N))}\right) \tag{A.3}$$

The numerator is a 2-D complex-valued Gaussian distribution, which, using the correlation properties, become

$$f(r(k),r(k+N))=\frac{1}{\pi^2(\sigma_s^2+\sigma_n^2)^2(1-\rho^2)}\exp\left(-\frac{|r(k)|^2-2\rho\,\mathrm{Re}\{e^{j2\pi\varepsilon}r(k)r^*(k+N)\}+|r(k+N)|^2}{(\sigma_s^2+\sigma_n^2)(1-\rho^2)}\right) \tag{A.4}$$

The denominator consists of two 1-D complex Gaussian distributions

$$f(r(k))=\frac{1}{\pi(\sigma_s^2+\sigma_n^2)}\exp\left(-\frac{|r(k)|^2}{(\sigma_s^2+\sigma_n^2)}\right) \tag{A.5}$$

and the log-likelihood function , after some algebraic manipulations, becomes

$$\Lambda(\theta,\varepsilon)=c_1+c_2(|\gamma(\theta)|\cos(2\pi\varepsilon+\angle\gamma(\theta))-\rho\Phi(\theta)) \tag{A.6}$$

where c_1 and c_2 are constants, independent of θ and ε.

Since the maximizing argument of $\Lambda(\theta, \varepsilon)$ is independent of constants c_1 and c_2, and $c_2 > 0$. Therefore

$$\Lambda(\theta,\varepsilon)=|\gamma(\theta)|\cos(2\pi\varepsilon+\angle\gamma(\theta))-\rho\Phi(\theta) \tag{A.7}$$

where $\angle$ denotes the argument of a complex number.

$$\gamma(\theta)=\sum_{k=\theta}^{\theta+N_g-1}r(k)r^*(k+N) \tag{A.8}$$

$$\Phi(\theta)=\frac{1}{2}\sum_{k=\theta}^{\theta+N_g-1}|r(k)|^2+|r(k+N)|^2 \tag{A.9}$$

and

$$\rho\triangleq\left|\frac{E\{r(k)r^*(k+N)\}}{\sqrt{E\{|r(k)|^2\}E\{|r(k+N)|^2\}}}\right|$$

$$=\frac{\sigma_s^2}{\sigma_s^2+\sigma_n^2}$$

$$=\frac{SNR}{SNR+1} \tag{A.10}$$

is the magnitude of the correlation coefficient between *r(k)* and *r(k + N)*. The term $\gamma(\theta)$ is a sum of N_g consecutive correlations between pairs of samples spaced N samples apart, and the term $\Phi(\theta)$ is an energy term, independent of the frequency offset ε.

The maximization of the log-likelihood function can be performed in two steps:

$$\max_{(\theta,\varepsilon)} \Lambda(\theta,\varepsilon) = \max_{\theta} \max_{\varepsilon} \Lambda(\theta,\varepsilon) = \max_{\theta} \Lambda(\theta, \hat{\varepsilon}_{ML}(\theta)) \tag{A.11}$$

The maximum with respect to frequency offset ε is obtained when the cosine term in (A.7) equals one. This yields the ML estimation of ε.

$$\hat{\varepsilon}_{ML}(\theta) = -\frac{1}{2}\angle\gamma(\theta) + n \tag{A.12}$$

where n is an integer. Due to the periodicity of the cosine function, several maxima are found. We assume that an acquisition, or rough estimate, of the frequency offset has been performed and that $|\varepsilon| < 1/2$; thus $n = 0$. Since cosine term equals to unity, the log-likelihood function of θ (which is the compressed log-likelihood function with respect to ε) becomes

$$\Lambda(\theta, \hat{\varepsilon}_{ML}(\theta)) = |\gamma(\theta)| - \rho\Phi(\theta) \tag{A.13}$$

and the joint ML estimation of θ and ε becomes

$$\hat{\theta}_{ML} = \arg\max_{\theta}\{|\gamma(\theta)| - \rho\Phi(\theta)\} \tag{A.14}$$

$$\hat{\varepsilon}_{ML} = -\frac{1}{2\pi}\angle\gamma(\hat{\theta}_{ML}) \tag{A.15}$$

Notice that only two quantities affect the log-likelihood function i.e., the number of samples in the cyclic prefix N_g and the correlation coefficient ρ given by the *SNR*. If ε is a priori known to be zero, the log-likelihood function for θ becomes

$$\Lambda(\theta) = \mathrm{Re}\{\gamma(\theta)\} - \rho\Phi(\theta) \tag{A.16}$$

and $\hat{\theta}_{ML}$ is its maximizing argument [26].

Appendix B

Derivation of Symbol Time Offset Estimation for Both Cyclic Prefix and Pilot Symbols Based Scheme

Details of the derivation of the algorithm described in Section 3.1.3 is provided here. The log-likelihood function in (3.24) can be written as [23]

$$\Lambda(\theta) = \log \Pr[\mathbf{r}(.) = \mathrm{r}(.) \mid \theta]$$

$$= \log\left\{\prod_{k\in I}\Pr[\mathbf{r}(\mathbf{k}) = r(k), \mathbf{r}(\mathbf{k}+\mathbf{N}) = r(k+N)] \times \prod_{k\notin I\cup I'}\Pr[\mathbf{r}(\mathbf{k}) = r(k)]\right\}$$

$$= \log\left\{\prod_{k\in I}\frac{\Pr[\mathbf{r}(\mathbf{k}) = r(k), \mathbf{r}(\mathbf{k}+\mathbf{N}) = r(k+N)]}{\Pr[\mathbf{r}(\mathbf{k}) = r(k)]\Pr[\mathbf{r}(\mathbf{k}+\mathbf{N}) = r(k+N)]} \times \prod_{k}\Pr[\mathbf{r}(\mathbf{k}) = r(k)]\right\}$$

$$= \sum_{k\in I}\log\left\{\frac{\Pr[\mathbf{r}(\mathbf{k}) = r(k), \mathbf{r}(\mathbf{k}+\mathbf{N}) = r(k+N)]}{\Pr[\mathbf{r}(\mathbf{k}) = r(k)]\Pr[\mathbf{r}(\mathbf{k}+\mathbf{N}) = r(k+N)]}\right\} + \sum_{k}\log\Pr[\mathbf{r}(\mathbf{k}) = r(k)]. \tag{B.1}$$

The two-dimensional density $\Pr[\mathbf{r}(\mathbf{k}) = r(k), \mathbf{r}(\mathbf{k}+\mathbf{N}) = r(k+N)]$ is given by

$$\Pr[\mathbf{r}(\mathbf{k}) = r(k), \mathbf{r}(\mathbf{k}+\mathbf{N}) = r(k+N)]$$

$$= \frac{\exp\left(-\dfrac{|r(k)-m(k-\theta|^2 - 2\rho.\mathrm{Re}\{(r(k)-m(k-\theta))(r(k+N)-m(k+N-\theta))^*\} + |r(k+N)-m(k+N-\theta)|^2}{(\sigma_x^2+\sigma_n^2)(1-\rho^2)}\right)}{\pi^2(\sigma_x^2+\sigma_n^2)^2(1-\rho^2)} \tag{B.2}$$

where ρ is as defined in (3.27). The one-dimensional density $\Pr[\mathbf{r}(\mathbf{k}) = r(k)]$ in (B.1) is given by

$$\Pr[\mathbf{r}(\mathbf{k}) = r(k)] = \frac{1}{\pi(\sigma_x^2+\sigma_n^2)}\exp\left(-\frac{|r(k)-m(k-\theta)|^2}{(\sigma_x^2+\sigma_n^2)}\right). \tag{B.3}$$

In three steps, the first term in (B.1) is now calculated. First, submission of (B.2) and (B.3) yields a sum of a squared form. In the second step we expand and simplify this form by noting that

$$m(k-\theta) = m(k+N-\theta), \qquad k \in [\theta, \theta+N_g-1], \tag{B.4}$$

due to the cyclic prefix. In the third step we ignore the terms $\sum_{k=\theta}^{\theta+N_g-1}|m(k-\theta)|^2$ and $\sum_{k=\theta}^{\theta+N_g-1}\log(1-\rho^2)$ because they are constants and are not relevant to the maximizing argument of the log-likelihood function. Then the first term of (B.1) is proportional to

$$\sum_{k\in I}\log\left\{\frac{\Pr[\mathbf{r(k)}=r(k),\mathbf{r(k+N)}=r(k+N)]}{\Pr[\mathbf{r(k)}=r(k)]\Pr[\mathbf{r(k+N)}=r(k+N)]}\right\}$$

$$\propto \mathrm{Re}\left\{\sum_{k\in I}r(k)r^*(k+N)\right\}-\frac{\rho}{2}\sum_{k\in I}\left(|r(k)|^2+|r(k+N)|^2\right)-(1-\rho)\mathrm{Re}\left\{\sum_{k\in I}[r^*(k)+r^*(k+N)]m(k-\theta)\right\} \quad \text{(B.5)}$$

and the second term of (B.1) can be calculated in the similar way. Again by omitting some terms in the expansion which are independent of θ and do not affect the maximizing argument of the log-likelihood function, the log-likelihood function in (B.1) consists of the three terms in (B.5) and the additional term

$$\frac{1-\rho^2}{\rho}\mathrm{Re}\left\{\sum_k r(k)m^*(k-\theta)\right\}. \quad \text{(B.6)}$$

Now by using equations (B.5) and (B.6), the expression of (3.24) in section 3.1.3 can be obtained. i.e.,

$$\Lambda(\theta)=\rho\Lambda_{cp}(\theta)+(1-\rho)\Lambda_p(\theta) \quad \text{(B.7)}$$

where

$$\Lambda_{cp}(\theta)=\mathrm{Re}\left\{\sum_{k=\theta}^{\theta+N_g-1}r^*(k)r(k+N)\right\}-\frac{\rho}{2}\sum_{k=\theta}^{\theta+N_g-1}\left\{|r(k)|^2+|r(k+N)|^2\right\}$$

exploits the information contained in the redundancy due to the cyclic prefix in the received signal and

$$\Lambda_p(\theta)=(1+\rho)\mathrm{Re}\left\{\sum_k r^*(k)m(k-\theta)\right\}-\rho\,\mathrm{Re}\left\{\sum_{k=\theta}^{\theta+N_g-1}(r(k)+r(k+N))^*m(k-\theta)\right\}$$

exploits the information contained in the pilot symbols with correlation coefficient

$$\rho=\frac{\alpha\sigma_x^2}{\alpha\sigma_x^2+\sigma_n^2}=\frac{\alpha SNR}{\alpha SNR+1}.$$

Appendix C

MATLAB Codes for the Functions fade.m, delay.m and sefade.m

The following Matlab function code is written based on the equation (4.19). This function generates Rayleigh fading.

(C.1) *fade.m*

```
% fade.m
% generate rayleigh fade
function [iout,qout,ramp,rcos,rsin] = fade (idata,qdata,nsamp,tstp,fd,no,counter,flat)
% Input variables
% idata : input i channel data
% qdata : input q channel data
% nsamp : number of samples to be simulated
% tstp : minimum time resolution
% fd : maximum doppler frequency
% no : number of waves in order to generate fading

% counter : fading counter
% flat : flat fading or not
% (1-flat (only amplitude is fluctuated), 0-normal (phase and amplitude
% are fluctuated))
% Output variables
% iout : output i channel data
% qout : output q channel data
% ramp : amplitude contaminated by fading
% rcos : cosine value contaminated by fading
% rsin : sine value contaminated by fading
if fd ~= 0.0
ac0 = sqrt(1.0 ./ (2.0.*(no + 1)));
% power normalized constant (ich)
as0 = sqrt(1.0 ./ (2.0.*(no)));
```

```
% power normalized constant (qch)
ic0 = counter;
% fading counter
pai = 3.14159265;
wm = 2.0.*pai.*fd;
n = 4.*no + 2;
ts = tstp;
wmts = wm.*ts;
paino = pai./no;
xc=zeros(1,nsamp);
xs=zeros(1,nsamp);
ic=[1:nsamp]+ic0;
for nn = 1 : no
cwn = cos( cos(2.0.*pai.*nn./n).*ic.*wmts );
xc = xc + cos(paino.*nn).*cwn;

xs = xs + sin(paino.*nn).*cwn;
end
cwmt = sqrt(2.0).*cos(ic.*wmts);
xc = (2.0.*xc+cwmt).*ac0;
xs = 2.0.*xs.*as0;
ramp=sqrt(xc.^2+xs.^2);
rcos=xc./ramp;
rsin=xs./ramp;
if flat == 1
iout = sqrt(xc.^2 + xs.^2).*idata(1:nsamp);
% output signal (ich)
qout = sqrt(xc.^2 + xs.^2).*qdata(1:nsamp);
% output signal (qch)
else
iout = xc.*idata(1:nsamp) - xs.*qdata(1:nsamp);
% output signal (ich)
qout = xs.*idata(1:nsamp) + xc.*qdata(1:nsamp);
```

```
% output signal (qch)
end
else
iout=idata;
qout=qdata;
end
% end of file
```

The following function gives the delay to the input signal the simulation procedure is drawn in Figure (4.9).

(C.2) *delay.m*

```
% delay.m
% gives delay to input signal
function [iout,qout] = delay (idata,qdata,nsamp,idel)
% Input variables
% idata : input i channel data
% qdata : input q channel data
% nsamp : number of samples to be simulated
% idel : number of samples to be delayed
% Output variables
% iout : output i channel data
% qout : output q channel data
iout = zeros(1,nsamp);
qout = zeros(1,nsamp);
if idel ~= 0
iout(1:idel)=zeros(1,idel);
qout(1:idel)=zeros(1,idel);
end
iout(idel+1:nsamp)=idata(1:nsamp-idel);
qout(idel+1:nsamp)=qdata(1:nsamp-idel);
% end of file
```

This function generates frequency selecting fading

(C.3) *sefade.m*

```
% sefade.m
% generates frequency selecting fading
function[iout,qout,ramp,rcos,rsin]=sefade(idata,qdata,itau,dlvl,th,n0,itn,n1,nsamp,tst
p,fd,flat)
% Input variables
% idata : input i channel data
% qdata : input q channel data
% itau : delay time for each multipath fading

% dlvl : attenuation level for each multipath fading
% th : initialized phase for each multipath fading
% n0 : number of waves in order to generate each multipath fading
% itn : fading counter for each multipath fading
% n1 : number of summation for direct and delayed waves
% nsamp : total number of symbols
% tstp : minimum time resolution
% fd : maximum doppler frequency
% flat : flat fading or not
% (1-flat (only amplitude is fluctuated), 0-normal (phase and amplitude
% are fluctuated))
% Output variables
% iout : output i channel data
% qout : output q channel data
% ramp : amplitude contaminated by fading
% rcos : cosine value contaminated by fading
% rsin : sine value contaminated by fading
iout=zeros(1,nsamp);
qout=zeros(1,nsamp);
total_attn=sum(10.^(-1.0.*dlvl./10.0));
for k = 1 : n1
```

```
atts = 10.^( -0.05 .* dlvl(k));
if dlvl (k) == 40.0
atts = 0.0;
end
theta = th(k) .* pi ./ 180.0;
 [itmp,qtmp]=delay(idata,qdata,nsamp,itau(k));
[itmp3,qtmp3,ramp,rcos,rsin]=fade(itmp,qtmp,nsamp,tstp,fd,n0(k),itn(k),flat);
iout = iout + atts.*itmp3./sqrt(total_attn);
qout = qout + atts.*qtmp3./sqrt(total_attn);
end
% end of file
```